Electronic Supplementary Material (ESI) for Molecular Systems Design & Engineering.

Supporting Information

Mesoscale Artificial Synthesis of Conjugated Microporous Polymers

Catherine Mollart*, Bartosz Ciborowski and Abbie Trewin*

Contents

1. CMP-1

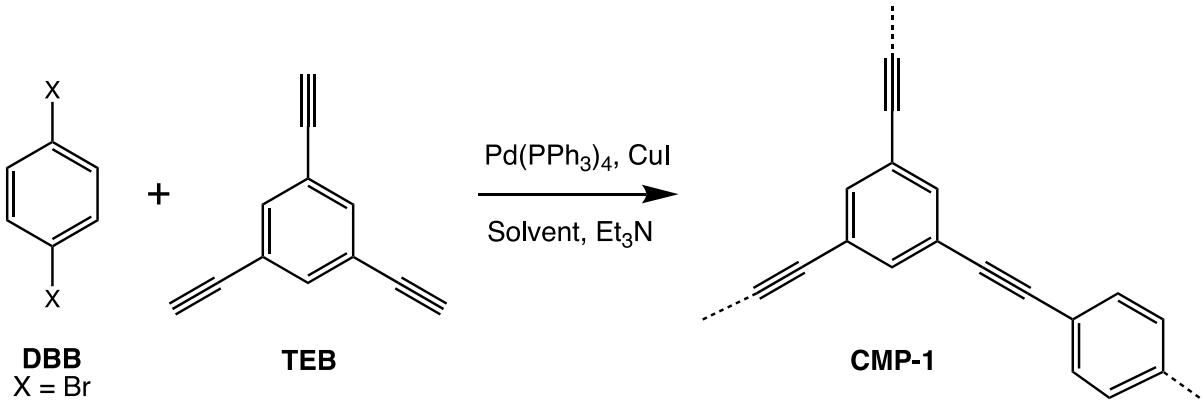

Figure S1. The reaction scheme used to synthesise CMP-1 from the reaction of 1,4-dibromobenzene (DBB) with 1,3,5-triethynylbenzene (TEB) in the presence of a $Pd(PPh_3)_4$ catalyst (cat), CuI co-catalyst, solvent, and triethylamine (TEA).

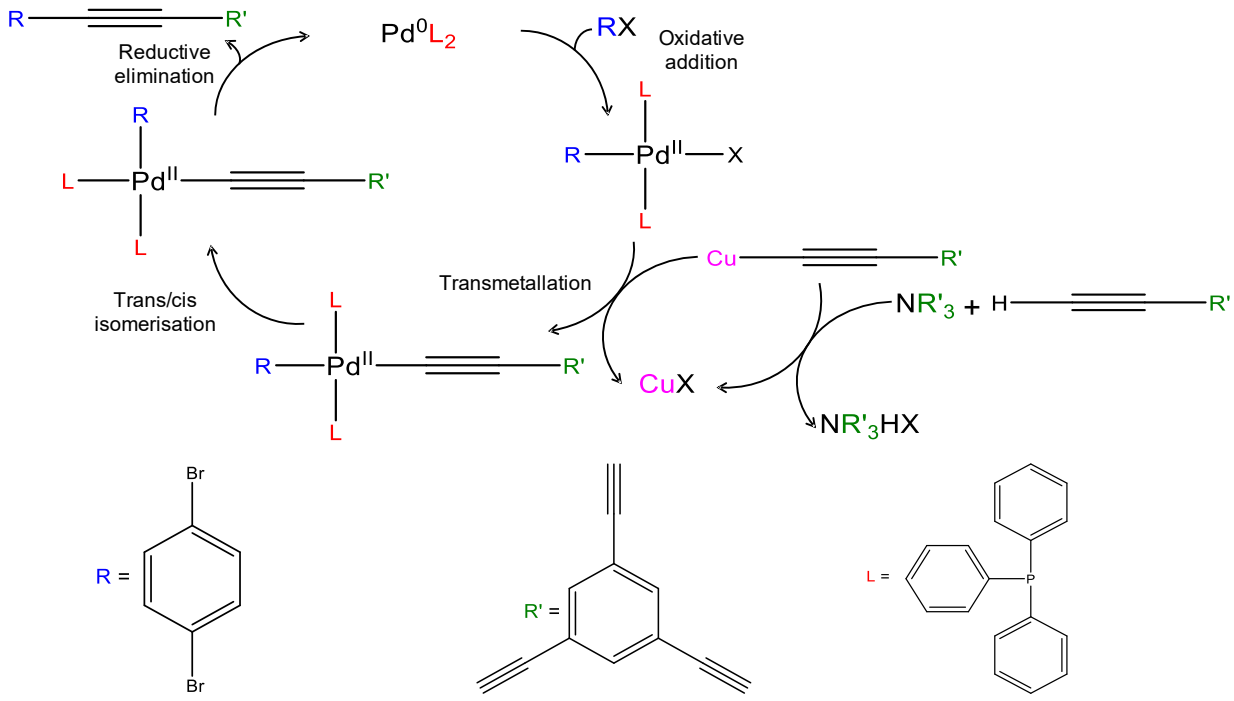

Figure S2. The Sonogashira–Hagihara catalytic cycle used to synthesise CMP-1. R – DBB, R' – TEB, L – triphenylphosphine. This consists of oxidative addition of DBB to the catalyst, transmetallation to substitute the bromine ligand with TEB, and reductive elimination of the cross-coupled product, regenerating the active catalyst. As discussed in our previous work,[1] we assume that the transmetallation side cycle has already occurred in our artificial synthesis protocol.

2. Ambuild

The structures simulated as part of this work were generated using the Ambuild code, which has been reported in detail elsewhere.[1-4] The methodology used in the artificial synthesis process is described as follows:

Network generation

The first step in the artificial synthesis is the generation of a simulation cell, which, unless otherwise specified, was set to (50 Å, 50 Å, 50 Å). To this cell, building blocks were seeded in the following quantities: cat–4, TEA–70, DBB–100, TEB–100, solvent (toluene unless otherwise specified)–130.

Following the seeding process, a loop is undertaken to incorporate the removal of unreacted DBB and TEB building blocks, geometry optimisation, and NVT (constant number of molecules, cell volume, and temperature) molecular dynamics (MD), before gradually re-seeding the building blocks into the cell. The delete and re-seed steps enable a larger degree of statistical sampling of the material. After re-seeding, the loop is concluded with a zip step, to allow any building blocks that meet the pre-determined bonding rules, bond distance and bond angle criteria to form a bond.

Bonding rules were specified whereby the two monomers were able to bond to the catalyst, and upon doing so, could bond to another monomer bonded to a catalyst molecule, breaking their respective bonds to the catalyst upon forming the new bonds.

Desolvation, homocoupling, workup and cell equilibration

The desolvation process, described as strategy 6 in reference 1, was designed to remove any unreacted solvent, TEA, and monomer/catalyst building blocks, incorporating NVT MD and geometry optimisation throughout. Following this, a new bond type is specified to enable homocoupling between TEB alkyne struts, which enhances the microporosity of the material by holding the polymer framework open, as first reported by Laybourn *et al.*[5] The structure then undergoes a workup stage to replace any unreacted copper end groups with hydrogen atoms. Finally, the cell volume is allowed to equilibrate using NPT MD (allowing the cell volume to change while keeping the pressure constant) to remove any unstable pore voids that would not occur in the real-world material.

3. Mapping building blocks

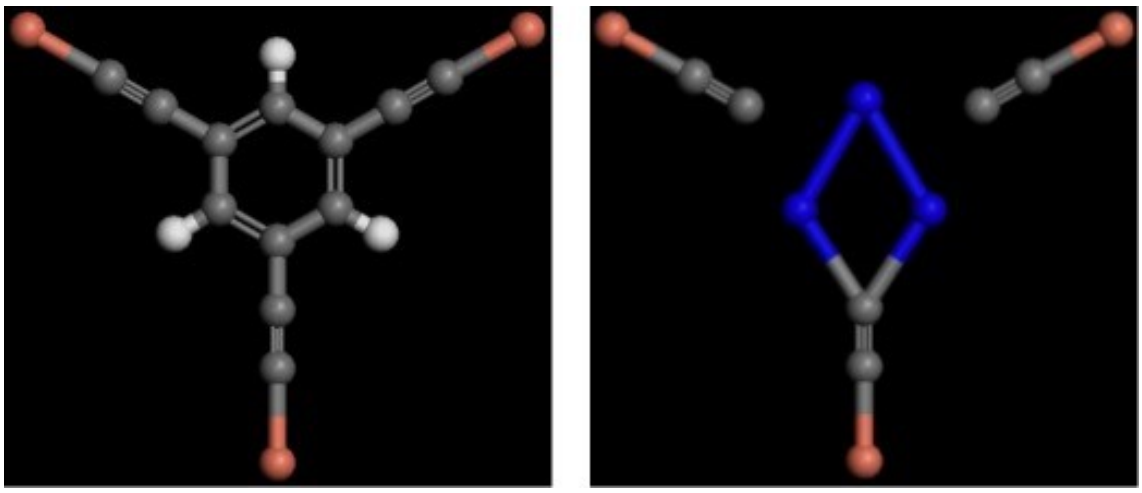

Figure S3. The all-atom (left) and hybrid coarse-grained (right) TEB blocks used in the artificial synthesis. Key: C – grey, H – white, Cu – orange, tBER grain – blue.

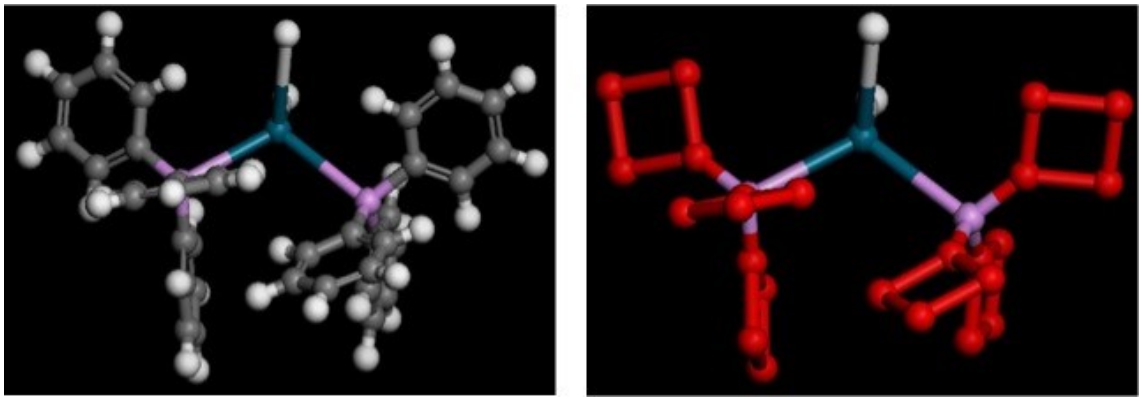

Figure S4. The all-atom (left) and hybrid coarse-grained (right) catalyst blocks used in the artificial synthesis. Key: C – grey, H – white, Pd – blue, P – purple, BER grain – red.

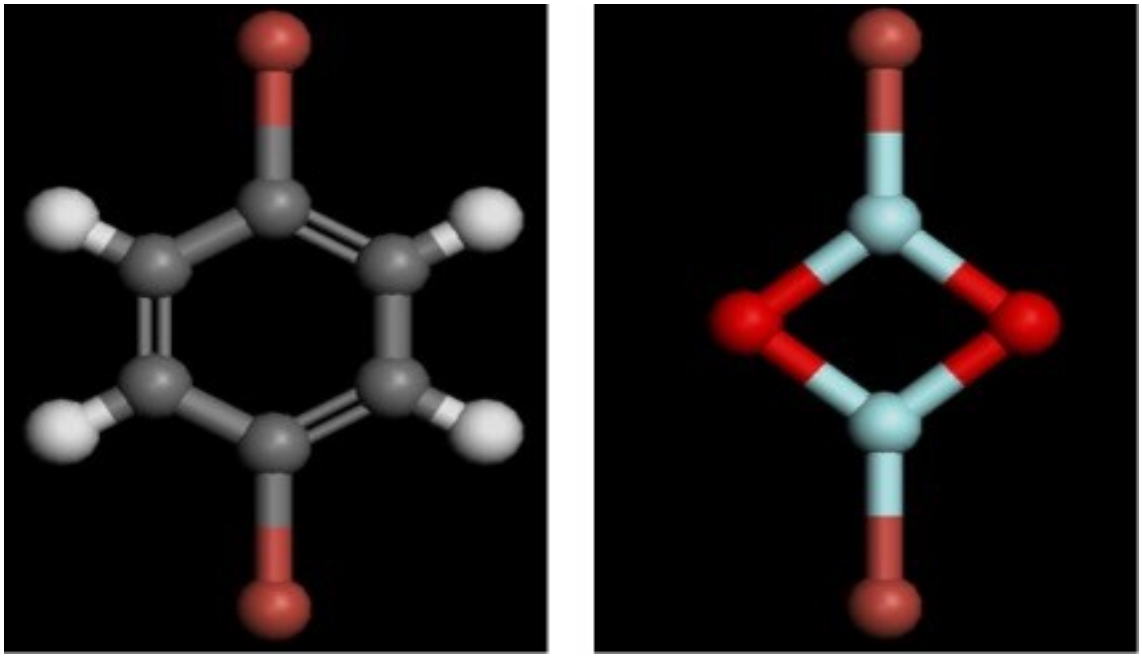

Figure S5. The all-atom (left) and hybrid coarse-grained (right) DBB blocks used in the artificial synthesis. Key: C – grey, H – white, Br – burgundy, dBER grain – pale blue, BER grain – red.

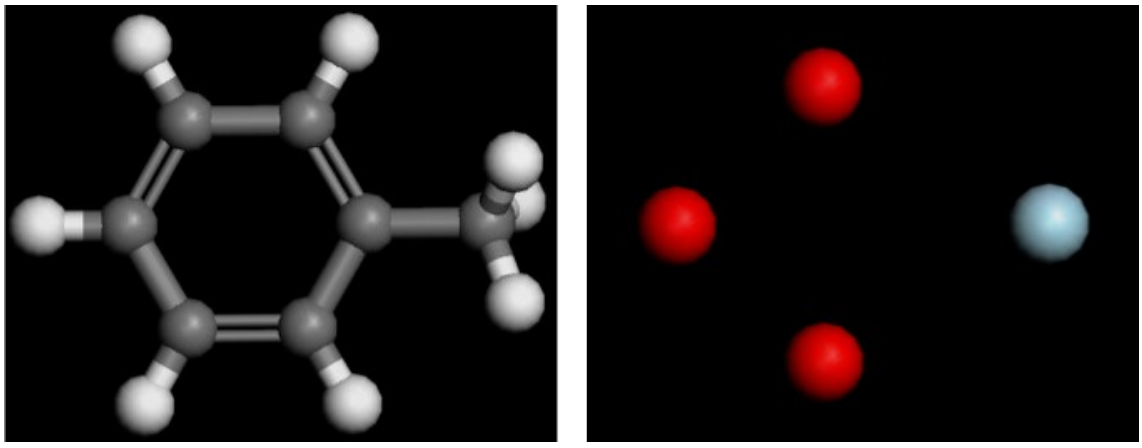

Figure S6. The all-atom (left) and coarse-grained (right) toluene blocks used in the artificial synthesis. Key: C – grey, H – white, XYR grain – pale blue, BER grain – red.

4. Fitting

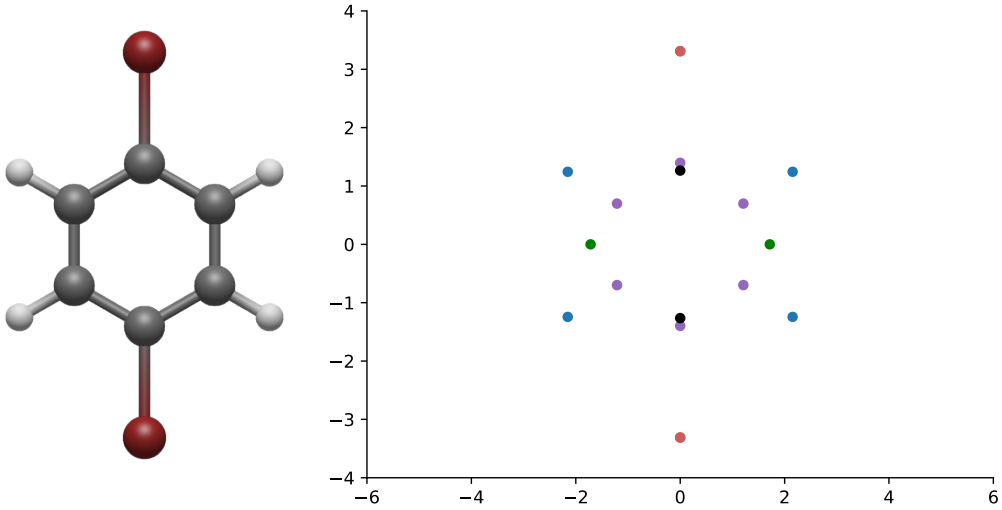

Figure S7. Left – DBB atomistic block (colour code as in Figure S5). Right – Fitting of the DBB hybrid coarse grain block to the atomistic. Key: Br – red, cp (aromatic) C – purple, H – blue, dBER grain – black, BER grain – green. The position, sigma, and epsilon values of the BER grain were shifted to better map to our atomistic block.

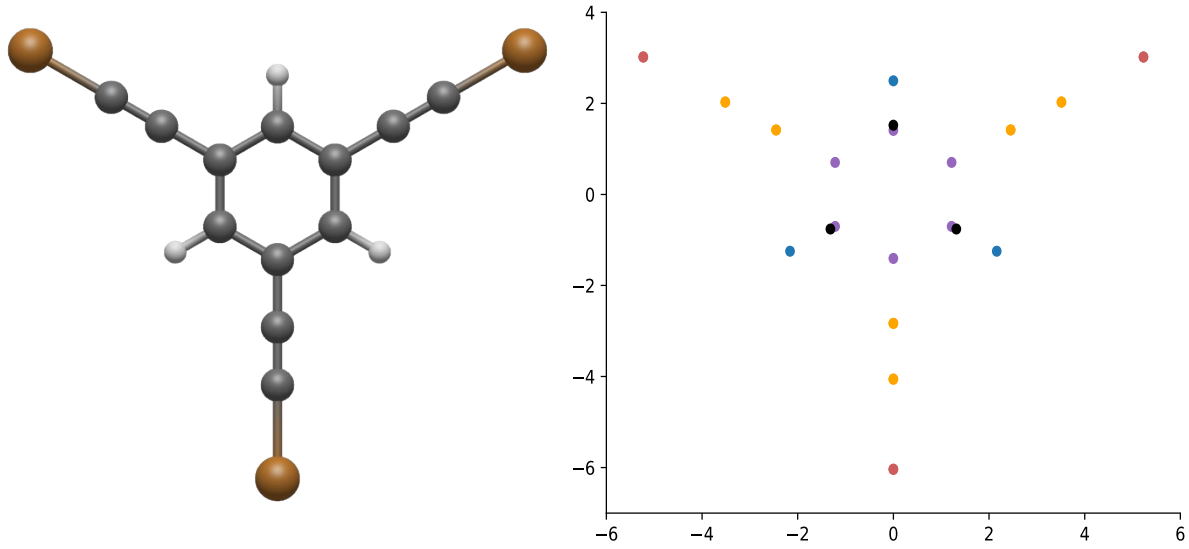

Figure S8. Left – TEB atomistic block (colour code as in Figure S3). Right – Fitting of the TEB hybrid coarse grain block to the atomistic. Key: Cu – red, cp (aromatic) C – purple, ct (*sp*-hybridised) C – yellow, H – blue, tBER grain – black.

Optimisation of the hybrid coarse grain fitting

The plots given below in Figures S9–10 show the superimposed hybrid coarse grain and all atom models of DBB or TEB given in Figures S7–8, along with sums of Lennard–Jones potentials calculated using the Lorentz–Berthelot mixing rules.[6, 7] A palladium reference atom is moved across the x axis (y = 0, z = 0) and the non-bonded interactions against all atoms in the model calculated.

By summing over all potentials of the reference atom against all atoms, we get a Lennard–Jones potential curve of a Pd atom as it approaches an all atom DBB or TEB molecule. By summing over all potentials of the reference atom against all grains, we get a Lennard–Jones potential curve of a Pd atom as it approaches a hybrid coarse grain molecule (this is described as a hybrid molecule due to the bromine atoms, which were included atomistically in our hybrid coarse grain models to act as Ambuild cap atoms, which are lost on forming the new bond between Ambuild end group atoms, as described in reference 1). By superimposing these several curves, we were able to observe the potential energy space around the all-atom and hybrid coarse grain models and compare the two.

Z_s is the value of shifting the entire molecule in the z axis. The reference atom is still moved along the x axis (y = 0, z = 0), so the Lennard–Jones potential space above/below the molecule is sampled.

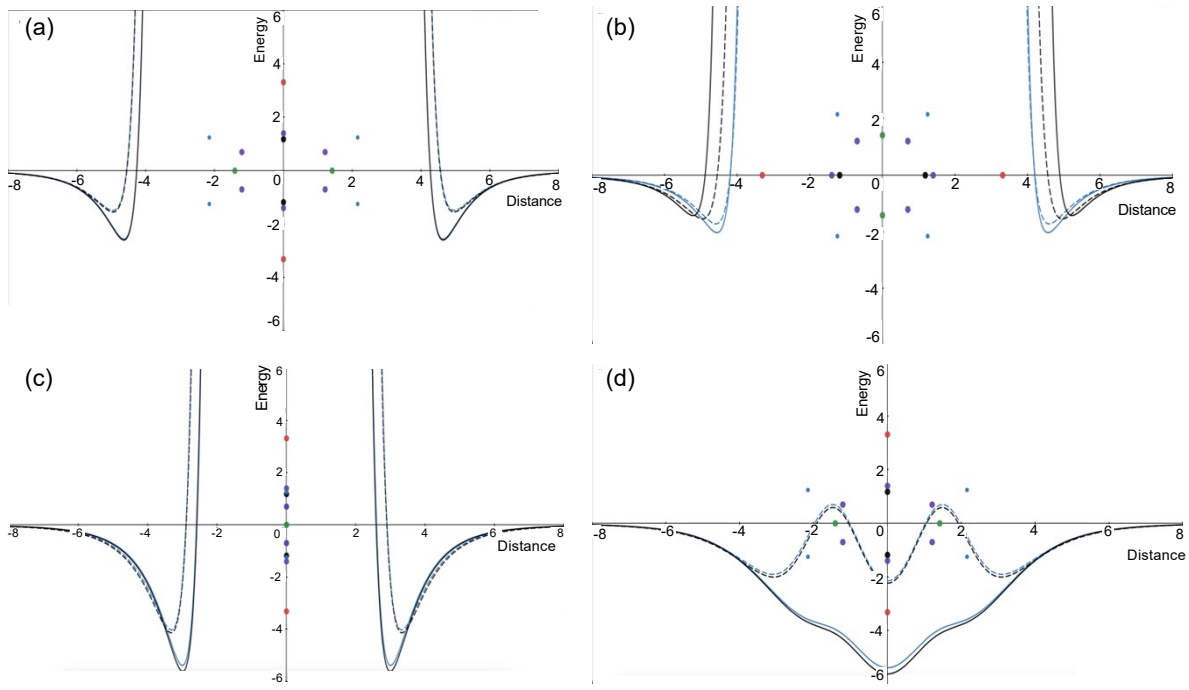

Figure S9. DBB grain fitting plots as described above. Key: all-atom DBB block with discarded Br atoms (as they're present in both our hybrid coarse grain and all-atom models) – solid blue line, DBB block with discarded Br atoms using our grains for the phenyl ring (alternating BER and dBER grains in a square) – dashed blue line, all-atom phenyl ring using the reference potentials[8] – solid black line, phenyl ring using the grains given in reference 8 (four BER grains in a square) – dashed black line, Br – red, cp (aromatic) C – purple, H – blue, dBER grain – black, BER grain – green. For all plots $\sigma = 3.7$ and $\varepsilon = 0.15713$. For (a), (b) and (c), $Z_s = 0$ and for (d) $Z_s = 3$. The bromine atoms are discarded as they remain an atom in all models, so we have not included the potential from the Br atoms in the potential fitting process.

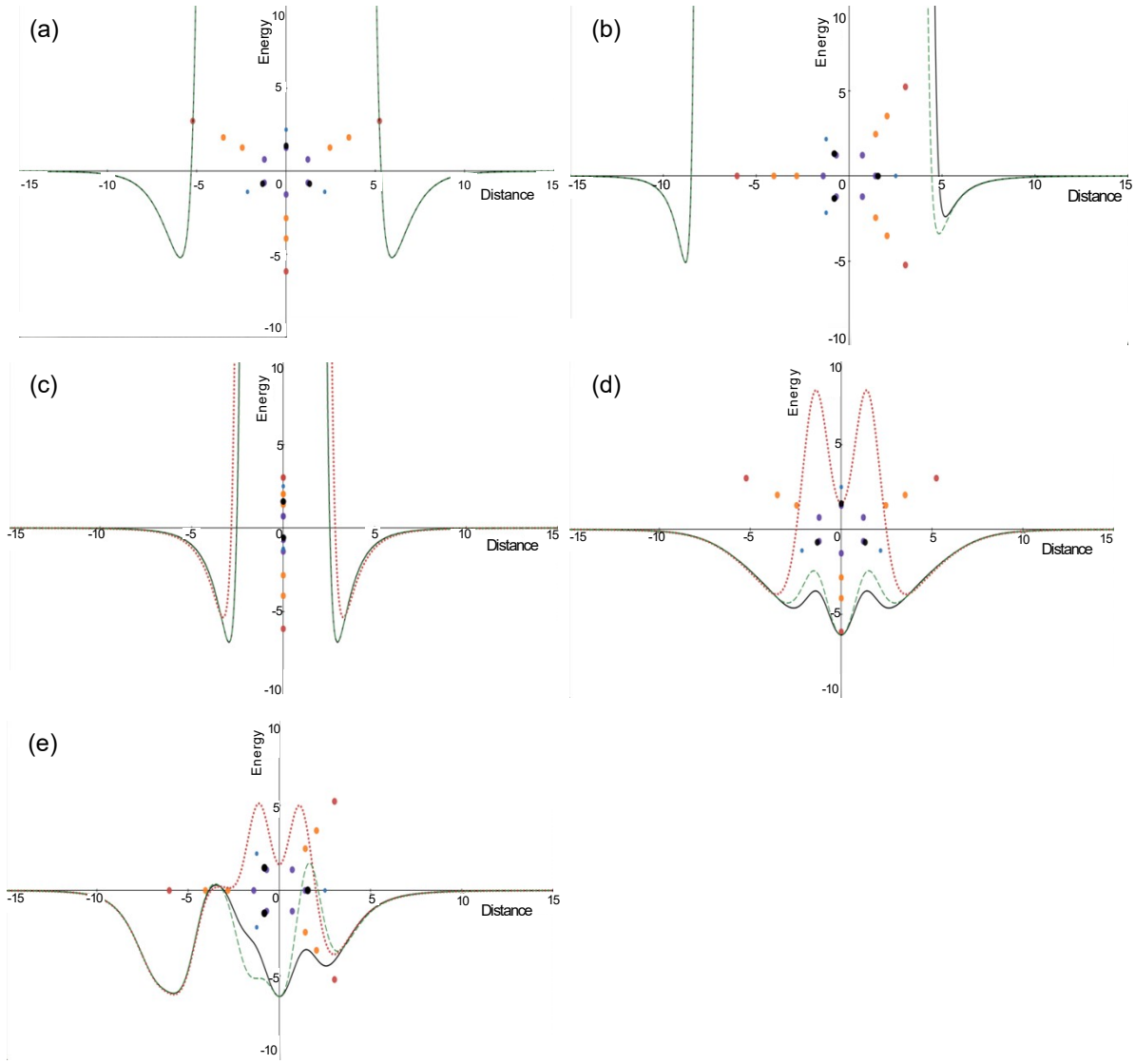

Figure S10. TEB grain fitting plots as described above. Key: all-atom TEB block – solid black line, TEB block using the reference grains[8] for the phenyl ring (four BER grains in a square) – dashed red line, TEB block using our grains for the phenyl ring (three tBER grains in a triangle) – dashed green line, Cu – red, cp (aromatic) C – purple, ct (*sp*-hybridised) C – yellow, H – blue, tBER grain – black. For all plots σ = 3.45 and ε = 0.5. For (a), (b) and (c), $Z_s = 0$ and for (d) and (e) $Z_s = 2.8$.

5. Parameters

Table S1. New bond parameters for the hybrid coarse grains discussed in this work, which were adapted from reference 8.

Bond	**k / kJ mol^{-1}**	**r_0 / Å**
BER-BER	800.0	2.00000
BER-XYR	800.0	2.60000
BER-p	197.0	1.78860
BER-ct1	813.2	1.53880
BER-dBER	800.0	1.84049
tBER-ct1	2000	2.45558
dBER-dBER	956.8	1.82438
dBER-ct2	213.2	1.65669
dBER-br	539.2	2.13219
dBER-Pd	700.0	3.45419

Table S2. New angle parameters for the hybrid coarse grains discussed in this work, which were adapted from reference 8.

Angle	k / kJ mol^{-1}	Theta / °
BER-BER-BER	300.0	90.00
BER-XYR-BER	300.0	58.00
XYR-BER-BER	300.0	106.00
p-BER-BER	113.0	135.00
BER-p-Pd	113.0	109.40
BER-p-BER	113.0	109.40
BER-p-Pd	113.0	109.40
BER-dBER-br	300.0	129.81
BER-dBER-BER	300.0	100.39
dBER-BER-dBER	300.0	79.60
tBER-ct1-ct2	113.0	147.13
tBER-ct1-tBER	131.8	174.25
ct1-tBER-ct1	131.8	65.75
BER-dBER-Pd	113.0	129.81
dBER-Pd-p	113.0	109.50
dBER-Pd-hcat	113.0	109.50
BER-dBER-ct2	131.8	129.81
dBER-ct2-ct1	113.0	179.46
dBER-Pd-dBER	113.0	109.50
dBER-Pd-ct2	113.0	109.50
BER-dBER-dBER	113.0	129.81

Table S3. New dihedral parameters for the hybrid coarse grains discussed in this work, which were adapted from reference 8. d and n are dimensionless.

Dihedral	k / kJ mol^{-1}	d	n	Dihedral	k / kJ mol^{-1}	d	n
BER-BER-BER-XYR	10	-1	1	Cu-ct2-ct1-tBER	0	1	2
XYR-BER-BER-BER	10	-1	1	tBER-ct1-ct2-Cu	0	1	2
BER-BER-XYR-BER	10	-1	1	BER-dBER-Pd-hcat	10	-1	2
BER-XYR-BER-BER	10	-1	1	hcat-Pd-dBER-BER	10	-1	2
br-dBER-BER-dBER	10	1	1	BER-dBER-Pd-p	10	-1	2
dBER-BER-dBER-br	10	1	1	p-Pd-dBER-BER	10	-1	2
dBER-BER-dBER-BER	10	-1	1	dBER-Pd-p-BER	10	-1	2
BER-dBER-BER-dBER	10	-1	1	BER-p-Pd-dBER	10	-1	2
BER-BER-BER-BER	10	-1	1	Pd-dBER-BER-dBER	10	-1	2
BER-BER-BER-p	10	1	1	dBER-BER-dBER-Pd	10	-1	2
p-BER-BER-BER	10	1	1	ct2-Pd-p-BER	10	1	2
BER-BER-p-BER	10	-1	2	BER-p-Pd-ct2	10	1	2
BER-p-BER-BER	10	-1	2	Pd-ct2-ct1-tBER	0	-1	1
BER-p-Pd-p	10	1	2	tBER-ct1-ct2-Pd	0	-1	1
p-Pd-p-BER	10	1	2	ct2-dBER-BER-dBER	7	-1	2
BER-p-Pd-hcat	10	1	2	dBER-BER-dBER-ct2	7	-1	2
hcat-Pd-p-BER	10	1	2	BER-dBER-ct2-ct1	0	-1	2
BER-BER-p-Pd	10	1	2	ct1-ct2-dBER-BER	0	-1	2
Pd-p-BER-BER	10	1	2	tBER-ct1-ct2-dBER	0	-1	2
ct2-ct1-tBER-ct1	10	1	1	dBER-ct2-ct1-tBER	0	-1	2
ct1-tBER-ct1-ct2	10	1	1	ct2-ct2-ct1-tBER	10	-1	2
ct1-tBER-ct1-tBER	10	-1	1	tBER-ct1-ct2-ct2	10	-1	2
tBER-ct1-tBER-ct1	10	-1	1	dBER-BER-dBER-dBER	7	-1	2
dBER-Pd-dBER-BER	10	-1	2	dBER-dBER-BER-dBER	7	-1	2

BER-dBER-Pd-dBER	10	-1	2	ct1-ct2-Pd-ct2	0	-1	1
BER-dBER-Pd-ct2	10	-1	2	ct2-Pd-ct2-ct1	0	-1	1
ct2-Pd-dBER-BER	10	-1	2	dBER-Pd-ct2-ct1	0	-1	1
BER-dBER-dBER-BER	7	-1	2	ct1-ct2-Pd-dBER	0	-1	1

Table S4. New non-bonding pair parameters for the hybrid coarse grains discussed in this work, which were adapted from reference 8. Every unlike pair potential was derived from like parameters *via* the Lorentz–Berthelot mixing rules.[7,8] All parameters were recalculated to a Lennard–Jones 12-6 from a 9-6 potential, so that the position (and magnitude) of the potential minimum is identical for all.

Atom 1	Atom 2	Epsilon	Sigma	Atom 1	Atom 2	Epsilon	Sigma
BER	BER	0.17500	3.87533	dBER	br	0.23414	3.76543
BER	XYR	0.23664	3.97732	dBER	Cu	0.77462	3.04269
BER	br	0.24710	3.85310	dBER	ct1	0.10028	3.63625
BER	Cu	0.81748	3.13036	dBER	ct2	0.10028	3.63625
BER	ct1	0.10583	3.72392	dBER	cp	0.13183	3.53095
BER	ct2	0.10583	3.72392	dBER	Pd	0.97779	3.13334
BER	cp	0.13912	3.61861	dBER	p	0.18380	3.76320
BER	Pd	1.03189	3.22101	dBER	na	0.10106	3.66298
BER	p	0.19397	3.85087	dBER	n3m	0.10106	3.66298
BER	na	0.10665	3.75065	dBER	c2	0.12108	3.53095
BER	n3m	0.10665	3.75065	dBER	c3	0.12108	3.53095
BER	c2	0.12778	3.61861	dBER	c4	0.12108	3.53095
BER	c3	0.12778	3.61861	dBER	hc	0.05606	3.18412
BER	c4	0.12778	3.61861	dBER	h1	0.05606	3.18412
BER	hc	0.05916	3.27179	dBER	h	0.05606	3.18412
BER	h1	0.05916	3.27179	dBER	hcat	0.00000	3.18412
BER	h	0.05916	3.27179	dBER	o1=	0.09710	3.42466
BER	hcat	0.00000	3.27179	tBER	tBER	0.50000	3.45000
BER	o1=	0.10247	3.51233	tBER	BER	0.29580	3.66267
XYR	XYR	0.32000	4.07930	tBER	XYR	0.40000	3.76465
XYR	br	0.33414	3.95508	tBER	br	0.41767	3.64043
XYR	Cu	1.10543	3.23234	tBER	Cu	1.38179	2.91769
XYR	ct1	0.14311	3.82590	tBER	ct1	0.17889	3.51125
XYR	ct2	0.14311	3.82590	tBER	ct2	0.17889	3.51125
XYR	cp	0.18813	3.72060	tBER	cp	0.23516	3.40595
XYR	Pd	1.39538	3.32299	tBER	Pd	1.74422	3.00834
XYR	p	0.26230	3.95285	tBER	p	0.32787	3.63820
XYR	na	0.14422	3.85263	tBER	na	0.18028	3.53798
XYR	n3m	0.14422	3.85263	tBER	n3m	0.18028	3.53798
XYR	c2	0.17279	3.72060	tBER	c2	0.21599	3.40595

XYR	c3	0.17279	3.72060	tBER	c3	0.21599	3.40595
XYR	c4	0.17279	3.72060	tBER	c4	0.21599	3.40595
XYR	hc	0.08000	3.37377	tBER	hc	0.10000	3.05912
XYR	h1	0.08000	3.37377	tBER	h1	0.10000	3.05912
XYR	h	0.08000	3.37377	tBER	h	0.10000	3.05912
XYR	hcat	0.00000	3.37377	tBER	hcat	0.00000	3.05912
dBER	dBER	0.15713	3.70000	tBER	o1=	0.17321	3.29966
dBER	BER	0.16582	3.78767	tBER	dBER	0.28029	3.57500
dBER	XYR	0.22424	3.88965				

6. Reaction comparison

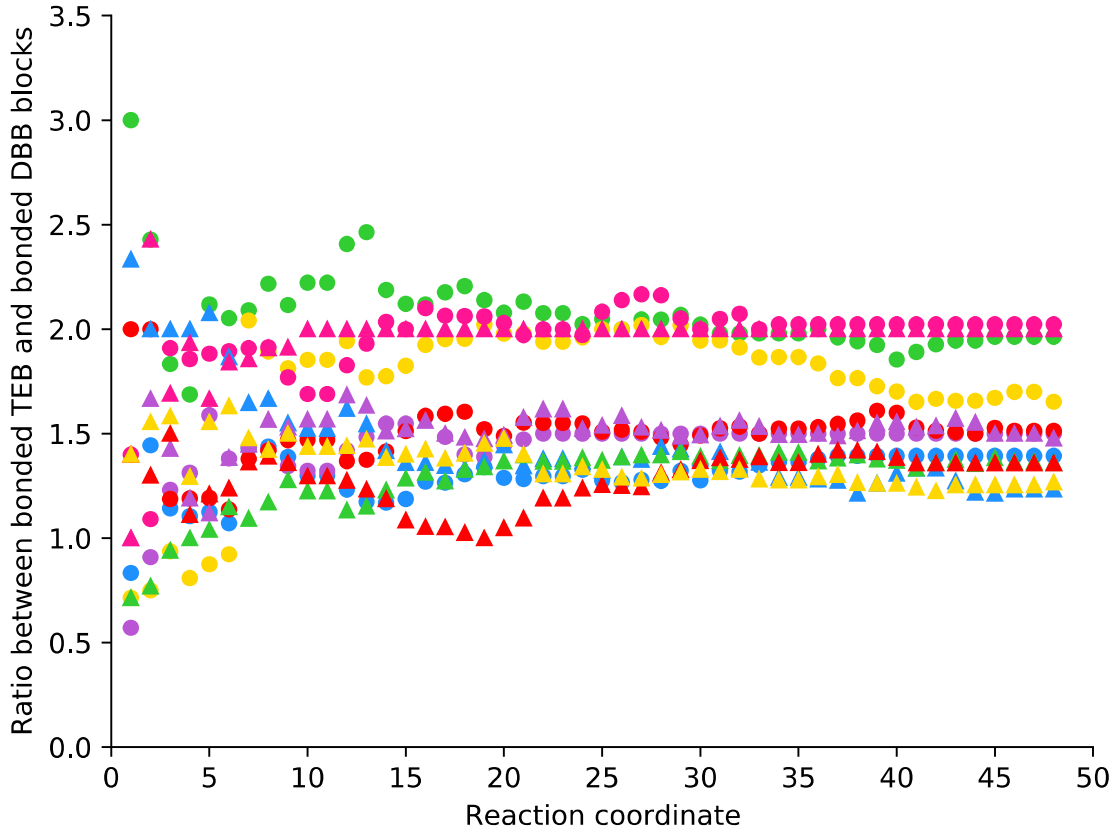

Figure S11. Ratio between TEB and DBB blocks which have undergone bonding of any kind against the reaction coordinate. Key: hybrid coarse grain model 1 – blue circle, hybrid coarse grain model 2 – green circle, hybrid coarse grain model 3 – purple circle, hybrid coarse grain model 4 – red circle, hybrid coarse grain model 5 – yellow circle, hybrid coarse grain model 6 – pink circle, all atom model 1 – blue triangle, all atom model 2 – green triangle, all atom model 3 – purple triangle, all atom model 4 – red triangle, all atom model 5 – yellow triangle, all atom model 6 – pink triangle.

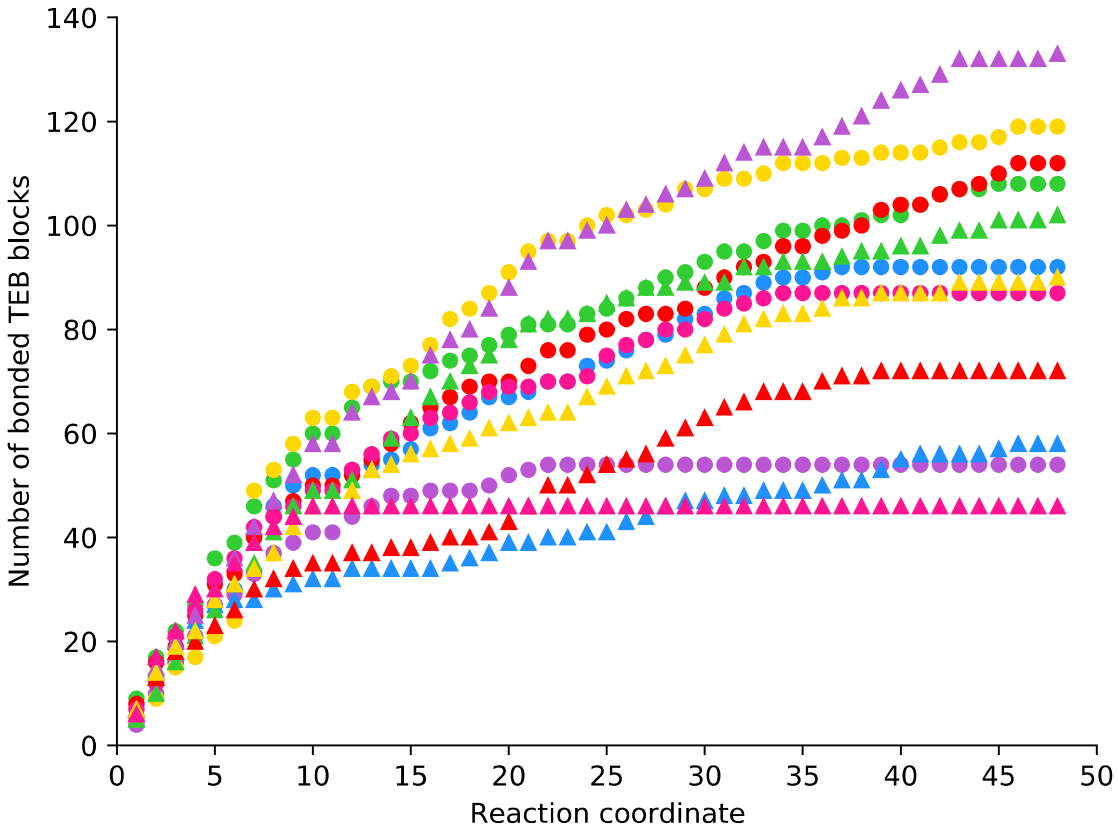

Figure S12. Number of TEB blocks which have undergone bonding of any kind against the reaction coordinate. Key: hybrid coarse grain model 1 – blue circle, hybrid coarse grain model 2 – green circle, hybrid coarse grain model 3 – purple circle, hybrid coarse grain model 4 – red circle, hybrid coarse grain model 5 – yellow circle, hybrid coarse grain model 6 – pink circle, all atom model 1 – blue triangle, all atom model 2 – green triangle, all atom model 3 – purple triangle, all atom model 4 – red triangle, all atom model 5 – yellow triangle, all atom model 6 – pink triangle.

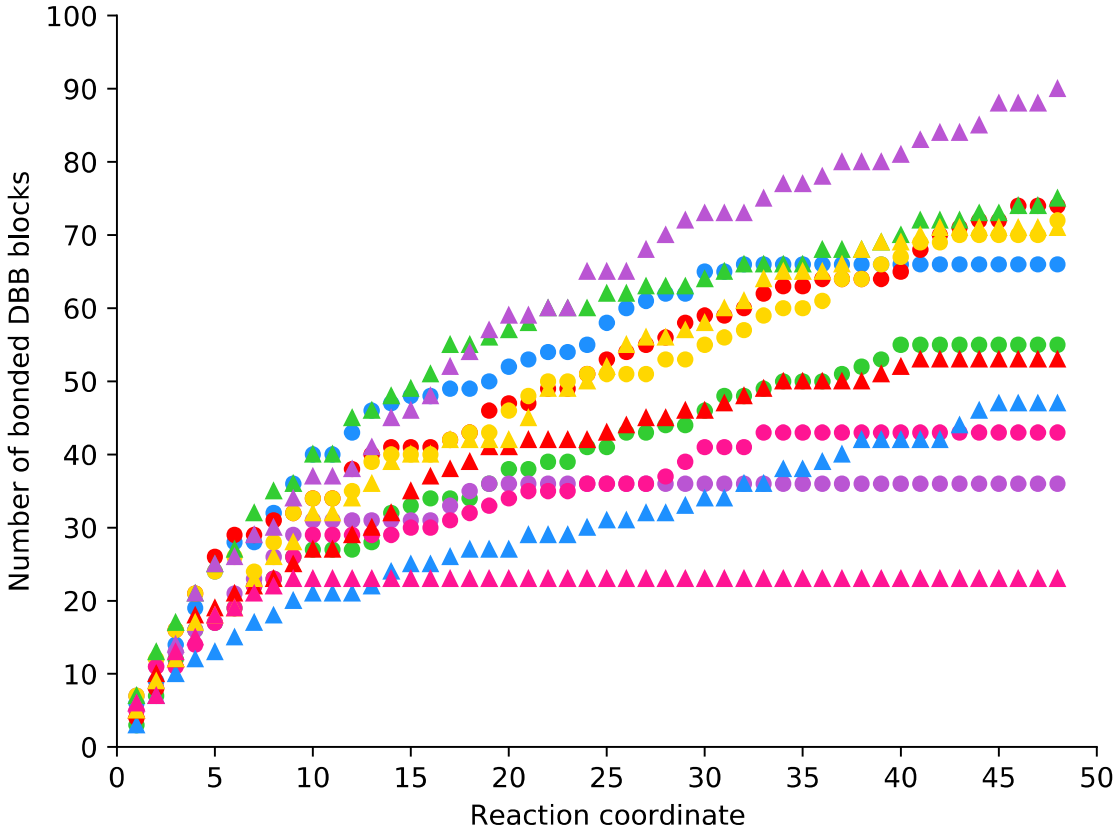

Figure S13. Number of DBB blocks which have undergone bonding of any kind against the reaction coordinate. Key: hybrid coarse grain model 1 – blue circle, hybrid coarse grain model 2 – green circle, hybrid coarse grain model 3 – purple circle, hybrid coarse grain model 4 – red circle, hybrid coarse grain model 5 – yellow circle, hybrid coarse grain model 6 – pink circle, all atom model 1 – blue triangle, all atom model 2 – green triangle, all atom model 3 – purple triangle, all atom model 4 – red triangle, all atom model 5 – yellow triangle, all atom model 6 – pink triangle.

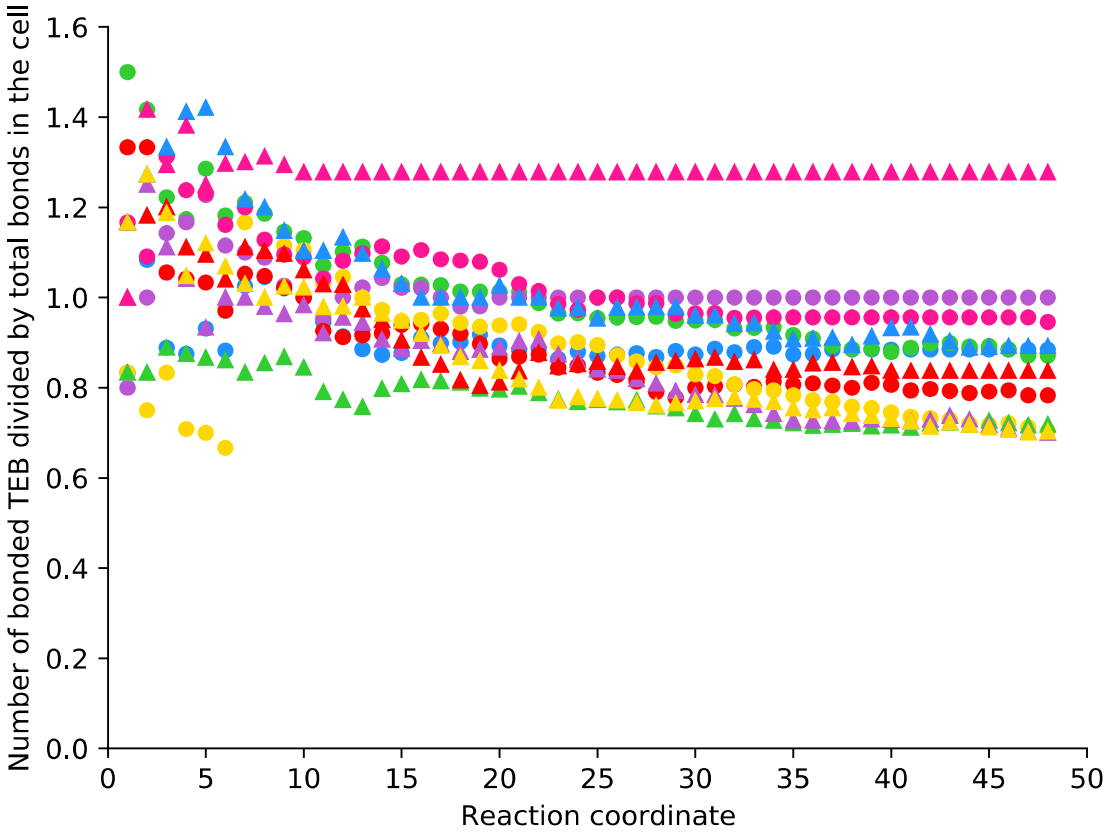

Figure S14. Number of TEB blocks which have undergone bonding of any kind divided by the total number of bonds against the reaction coordinate. Key: hybrid coarse grain model 1 – blue circle, hybrid coarse grain model 2 – green circle, hybrid coarse grain model 3 – purple circle, hybrid coarse grain model 4 – red circle, hybrid coarse grain model 5 – yellow circle, hybrid coarse grain model 6 – pink circle, all atom model 1 – blue triangle, all atom model 2 – green triangle, all atom model 3 – purple triangle, all atom model 4 – red triangle, all atom model 5 – yellow triangle, all atom model 6 – pink triangle.

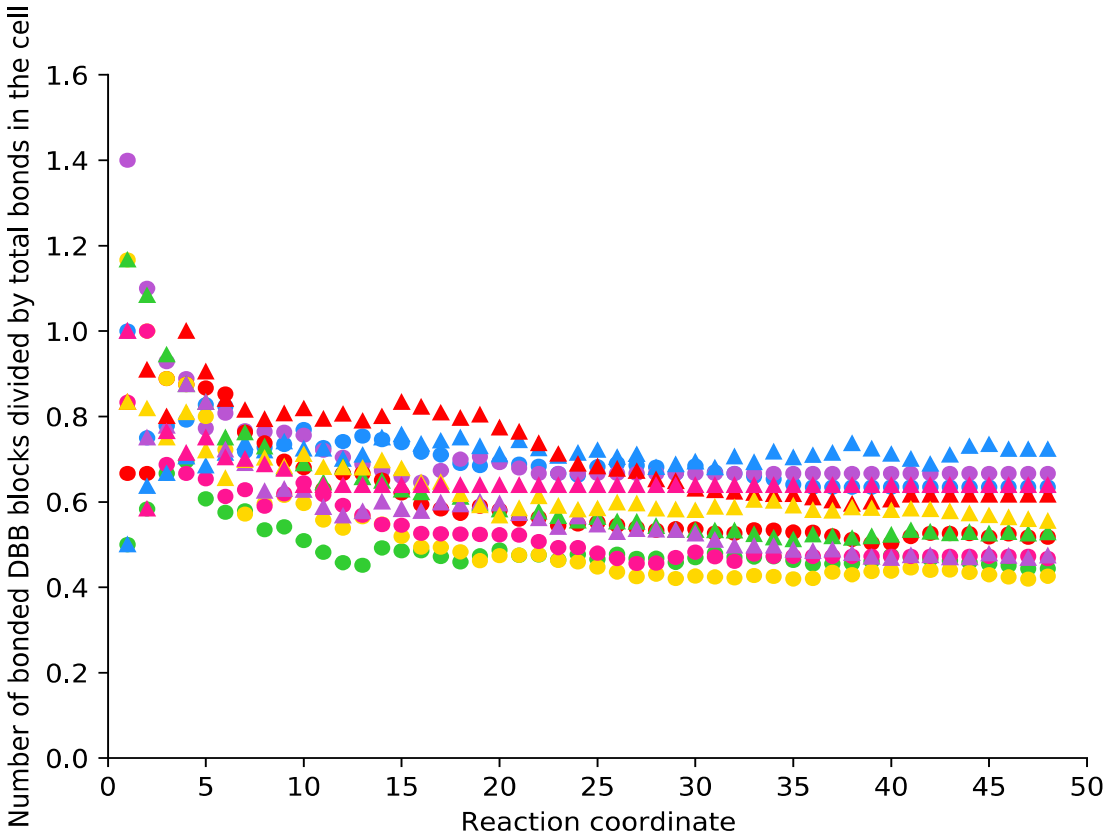

Figure S15. Number of DBB blocks which have undergone bonding of any kind divided by the total number of bonds against the reaction coordinate. Key: hybrid coarse grain model 1 – blue circle, hybrid coarse grain model 2 – green circle, hybrid coarse grain model 3 – purple circle, hybrid coarse grain model 4 – red circle, hybrid coarse grain model 5 – yellow circle, hybrid coarse grain model 6 – pink circle, all atom model 1 – blue triangle, all atom model 2 – green triangle, all atom model 3 – purple triangle, all atom model 4 – red triangle, all atom model 5 – yellow triangle, all atom model 6 – pink triangle.

7. Pair potential fitting

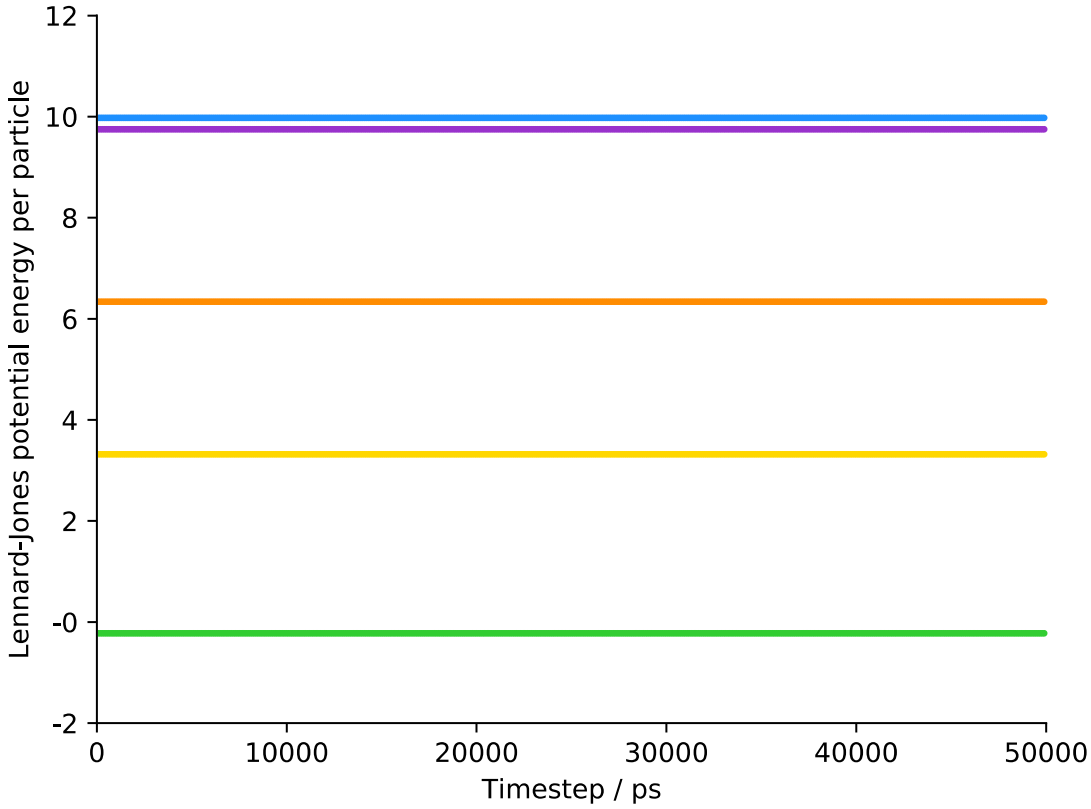

Figure S16. Plot of the average Lennard–Jones potential energy per particle as a function of the timestep across hybrid coarse-grain and all-atom models 1–4, artificially synthesised using toluene as the solvent. Key: all-atom – green, hybrid coarse grain with original pair potentials – orange, hybrid coarse grain with pair potential epsilon values x0.9 – purple, hybrid coarse grain with pair potential epsilon values x0.8 – yellow, hybrid coarse grain with pair potential epsilon values x0.7 – blue.

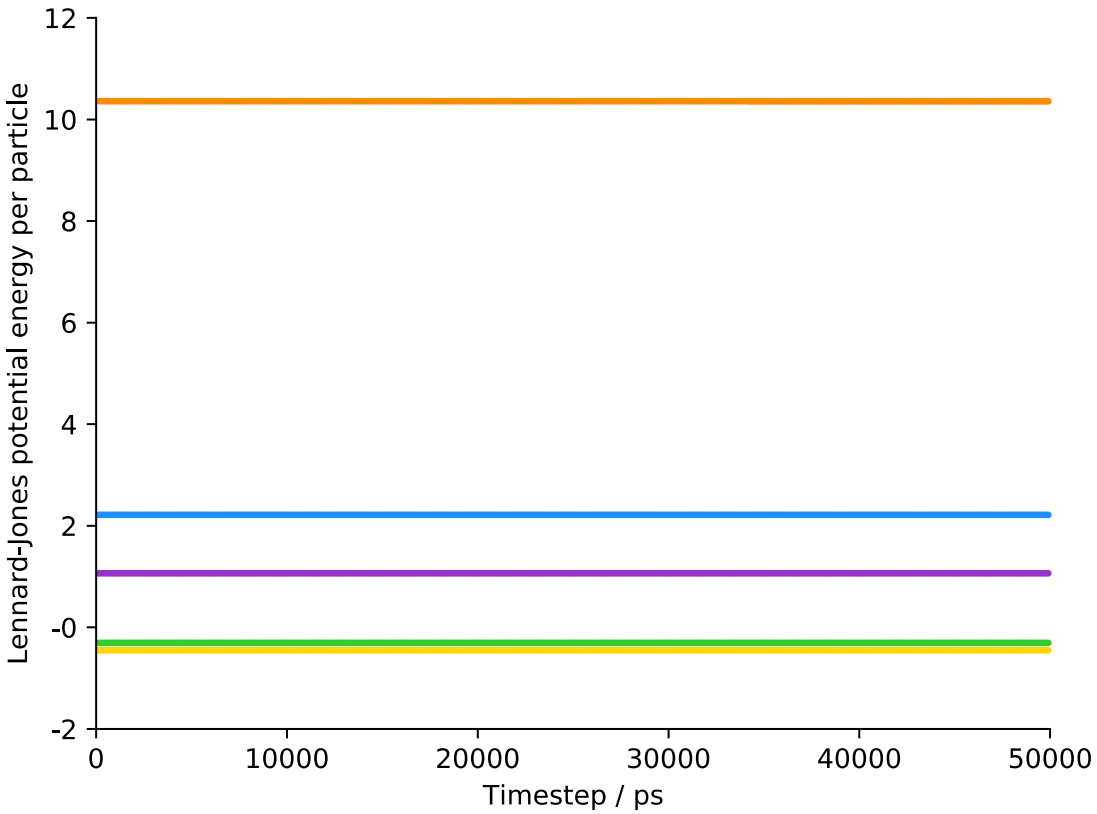

Figure S17. Plot of the average Lennard–Jones potential energy per particle as a function of the timestep across hybrid coarse-grain and all-atom models 1–4, artificially synthesised using DMF as the solvent. Key: all-atom – green, hybrid coarse grain with original pair potentials – orange, hybrid coarse grain with pair potential epsilon values x0.9 – purple, hybrid coarse grain with pair potential epsilon values x0.8 – yellow, hybrid coarse grain with pair potential epsilon values x0.7 – blue.

Table S5. Fitted non-bonding pair parameters for the hybrid coarse grains discussed in this work, which were adapted from reference 8. All pair potentials were taken from Table S4 and fitted so that the new epsilon value was 0.8x the original epsilon value calculated. The factor of 0.8 was chosen as this gave the closest potential energy of each respective hybrid coarse grain Lennard–Jones pair interaction to the all-atom equivalent (Figures S16–17). All sigma values remained unchanged from Table S4.

Atom 1	Atom 2	Epsilon	Sigma	Atom 1	Atom 2	Epsilon	Sigma
BER	BER	0.140000	3.87533	dBER	br	0.187312	3.76543
BER	XYR	0.189312	3.97732	dBER	Cu	0.619696	3.04269
BER	br	0.197680	3.85310	dBER	ct1	0.080224	3.63625
BER	Cu	0.653984	3.13036	dBER	ct2	0.080224	3.63625
BER	ct1	0.084664	3.72392	dBER	cp	0.105464	3.53095

BER	ct2	0.084664	3.72392	dBER	Pd	0.782232	3.13334
BER	cp	0.111296	3.61861	dBER	p	0.147040	3.76320
BER	Pd	0.825512	3.22101	dBER	na	0.080848	3.66298
BER	p	0.155176	3.85087	dBER	n3m	0.080848	3.66298
BER	na	0.085320	3.75065	dBER	c2	0.096864	3.53095
BER	n3m	0.085320	3.75065	dBER	c3	0.096864	3.53095
BER	c2	0.102224	3.61861	dBER	c4	0.096864	3.53095
BER	c3	0.102224	3.61861	dBER	hc	0.044848	3.18412
BER	c4	0.102224	3.61861	dBER	h1	0.044848	3.18412
BER	hc	0.047328	3.27179	dBER	h	0.044848	3.18412
BER	h1	0.047328	3.27179	dBER	hcat	0.000000	3.18412
BER	h	0.047328	3.27179	dBER	o1=	0.077680	3.42466
BER	hcat	0.000000	3.27179	tBER	tBER	0.400000	3.45000
BER	o1=	0.081976	3.51233	tBER	BER	0.236640	3.66267
XYR	XYR	0.256000	4.07930	tBER	XYR	0.320000	3.76465
XYR	br	0.267312	3.95508	tBER	br	0.334136	3.64043
XYR	Cu	0.884344	3.23234	tBER	Cu	1.105432	2.91769
XYR	ct1	0.114488	3.82590	tBER	ct1	0.143112	3.51125
XYR	ct2	0.114488	3.82590	tBER	ct2	0.143112	3.51125
XYR	cp	0.150504	3.72060	tBER	cp	0.188128	3.40595
XYR	Pd	1.116304	3.32299	tBER	Pd	1.395376	3.00834
XYR	p	0.209840	3.95285	tBER	p	0.262296	3.63820
XYR	na	0.115376	3.85263	tBER	na	0.144224	3.53798
XYR	n3m	0.115376	3.85263	tBER	n3m	0.144224	3.53798
XYR	c2	0.138232	3.72060	tBER	c2	0.172792	3.40595
XYR	c3	0.138232	3.72060	tBER	c3	0.172792	3.40595
XYR	c4	0.138232	3.72060	tBER	c4	0.172792	3.40595
XYR	hc	0.064000	3.37377	tBER	hc	0.080000	3.05912
XYR	h1	0.064000	3.37377	tBER	h1	0.080000	3.05912
XYR	h	0.064000	3.37377	tBER	h	0.080000	3.05912
XYR	hcat	0.000000	3.37377	tBER	hcat	0.000000	3.05912
dBER	dBER	0.125704	3.70000	tBER	o1=	0.138568	3.29966
dBER	BER	0.132656	3.78767	tBER	dBER	0.224232	3.57500
dBER	XYR	0.179392	3.88965				

8. Cell block analysis

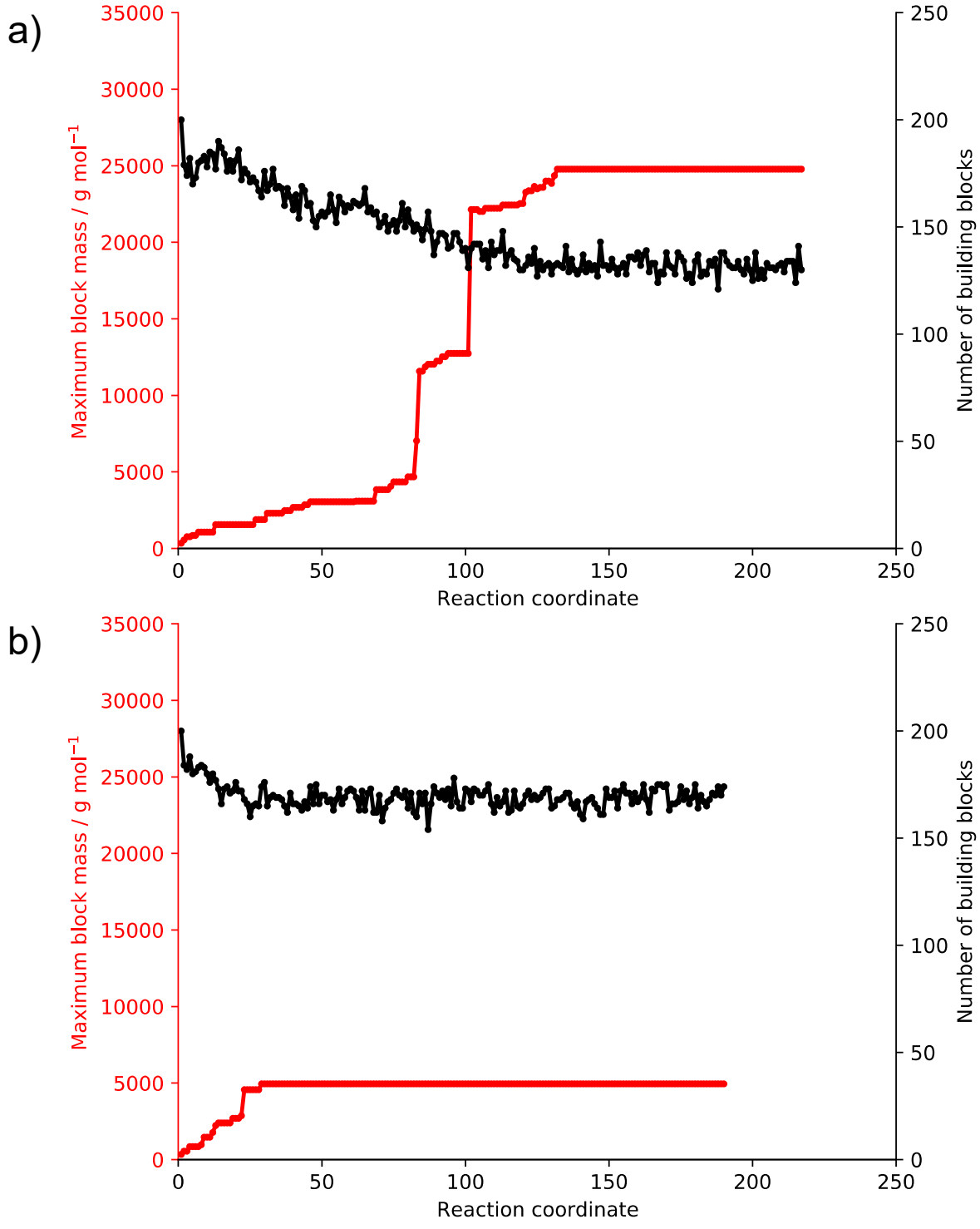

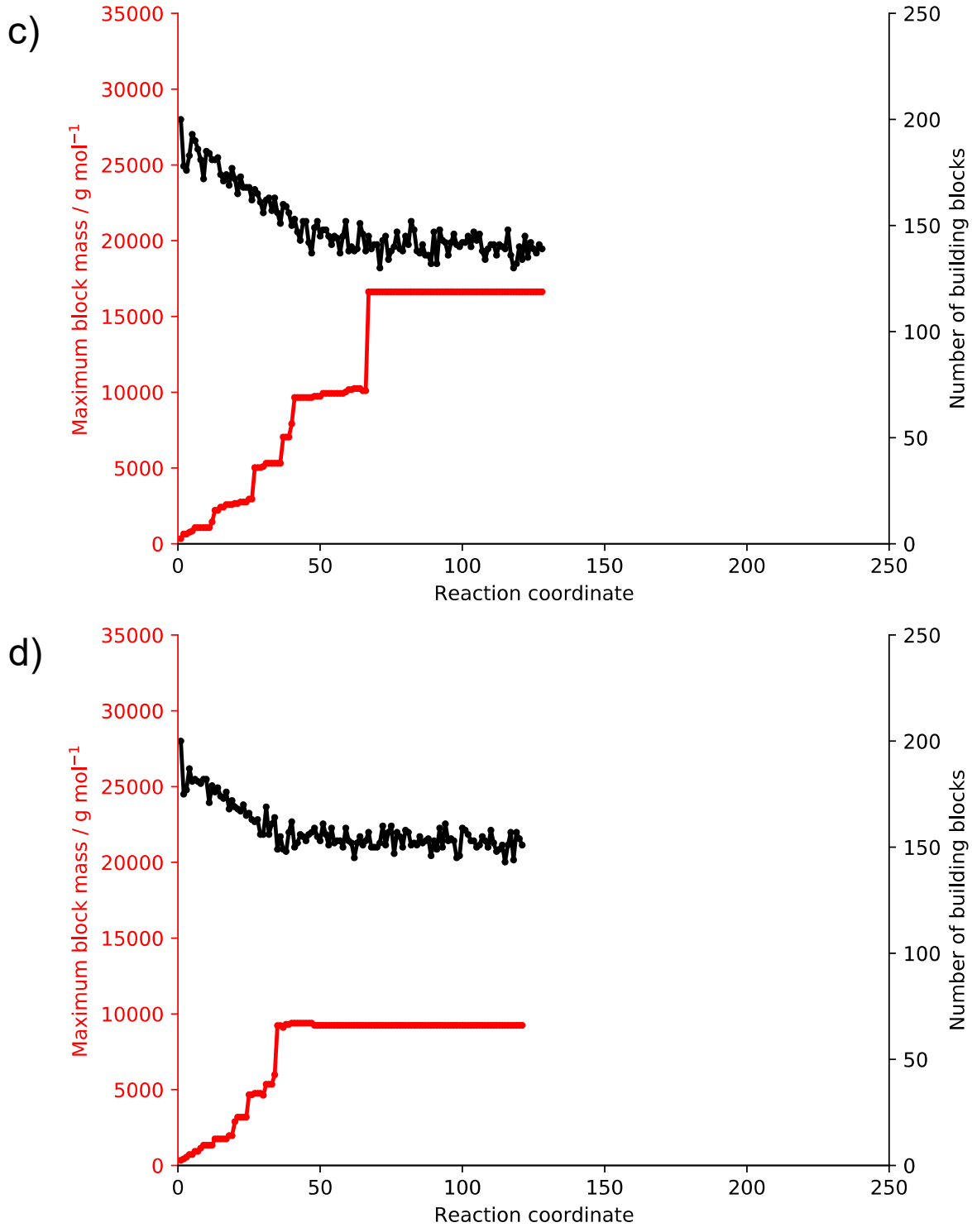

Figure S18. Plots of the maximum block size and number of blocks in the simulation cell against the reaction step for all-atom models 1–4, artificially synthesised using toluene as the solvent: a) model 1, b) model 2, c) model 3, d) model 4. Key: Number of building blocks – black, maximum block mass – red.

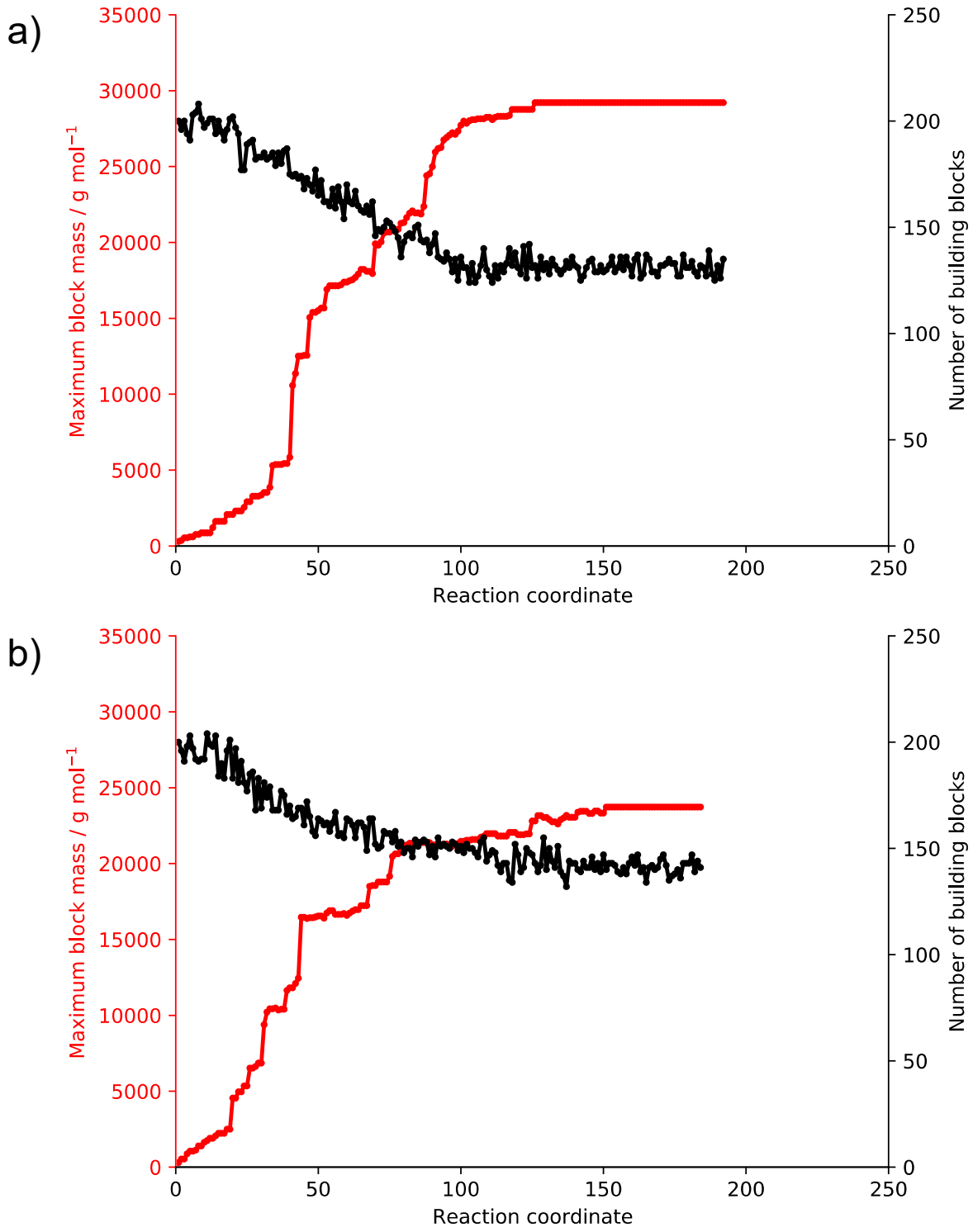
a)
Maximum block mass / g mol⁻¹
Number of building blocks
Reaction coordinate
0
5000
10000
15000
20000
25000
30000
35000
0
50
100
150
200
250
b)
Maximum block mass / g mol⁻¹
Number of building blocks
Reaction coordinate

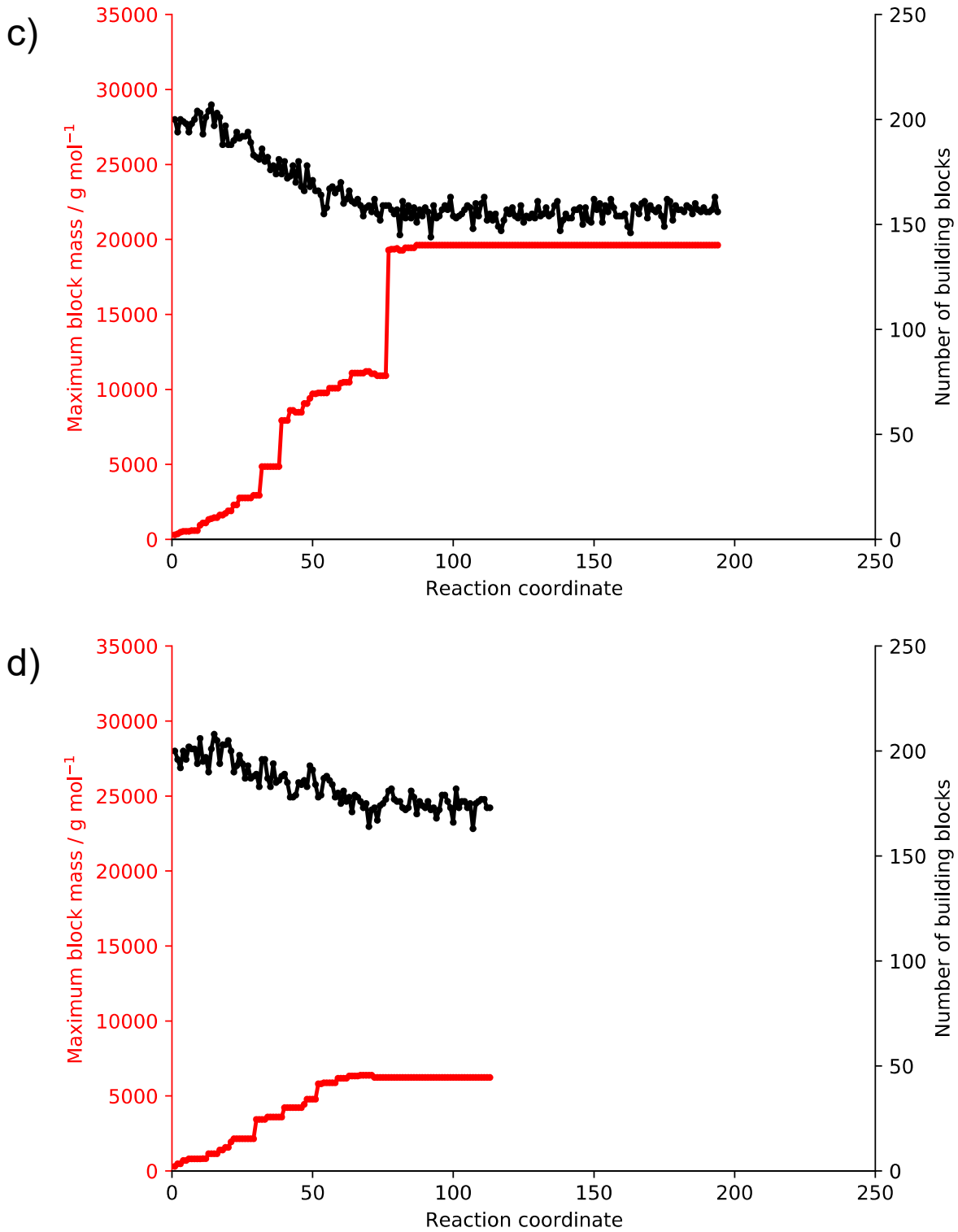

Figure S19. Plots of the maximum block size and number of blocks in the simulation cell against the reaction step for hybrid coarse-grain models 1–4, artificially synthesised using toluene as the solvent and using the fitted pair potentials given in Table S5: a) model 1, b) model 2, c) model 3, d) model 4. Key: Number of building blocks – black, maximum block mass – red.

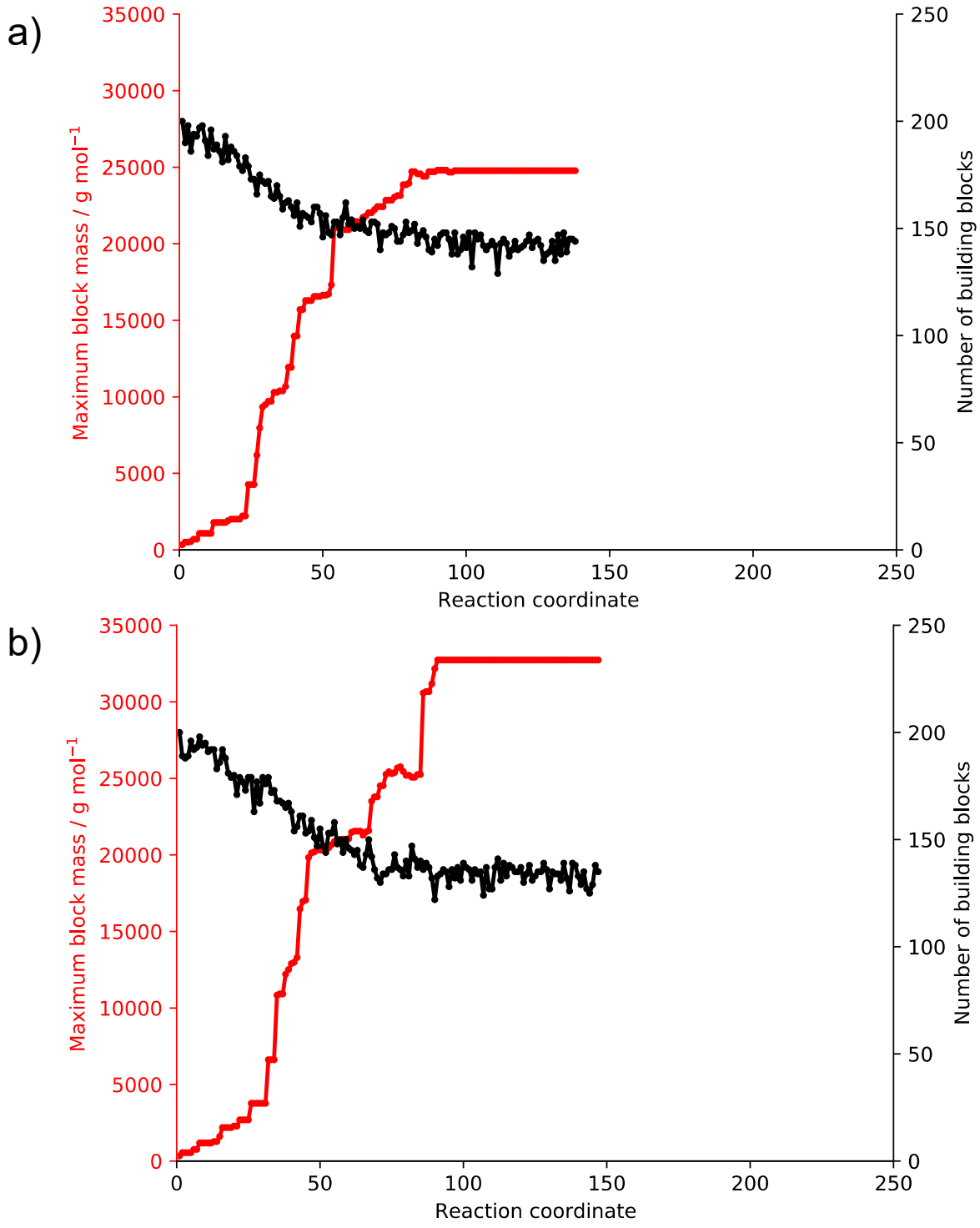
a)
Maximum block mass / g mol^{-1}
Number of building blocks
Reaction coordinate
0
5000
10000
15000
20000
25000
30000
35000
0
50
100
150
200
250
b)
Maximum block mass / g mol^{-1}
Number of building blocks
Reaction coordinate

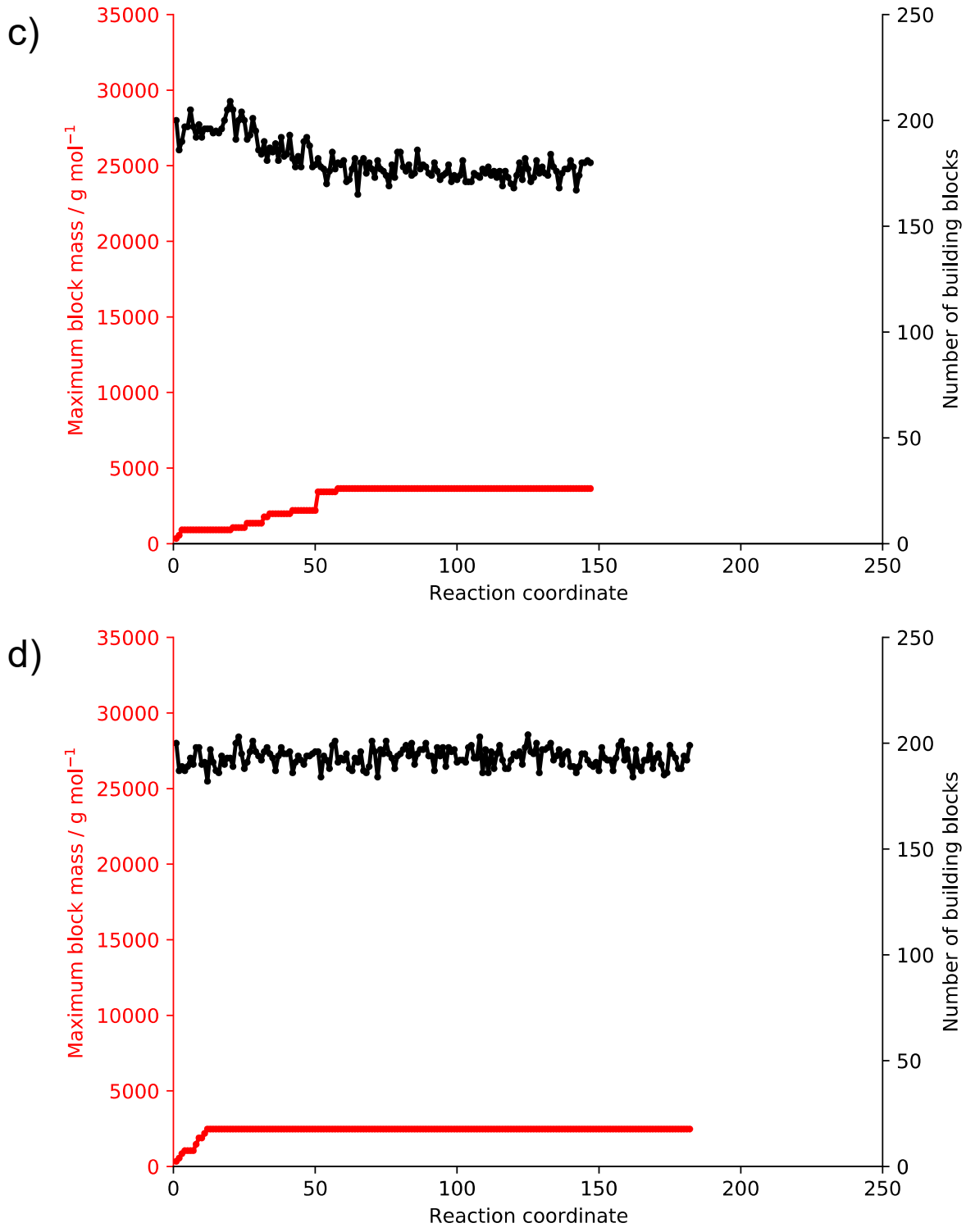

Figure S20. Plots of the maximum block size and number of blocks in the simulation cell against the reaction step for all-atom models 1–4, artificially synthesised using DMF as the solvent: a) model 1, b) model 2, c) model 3, d) model 4. Key: Number of building blocks – black, maximum block mass – red.

a)

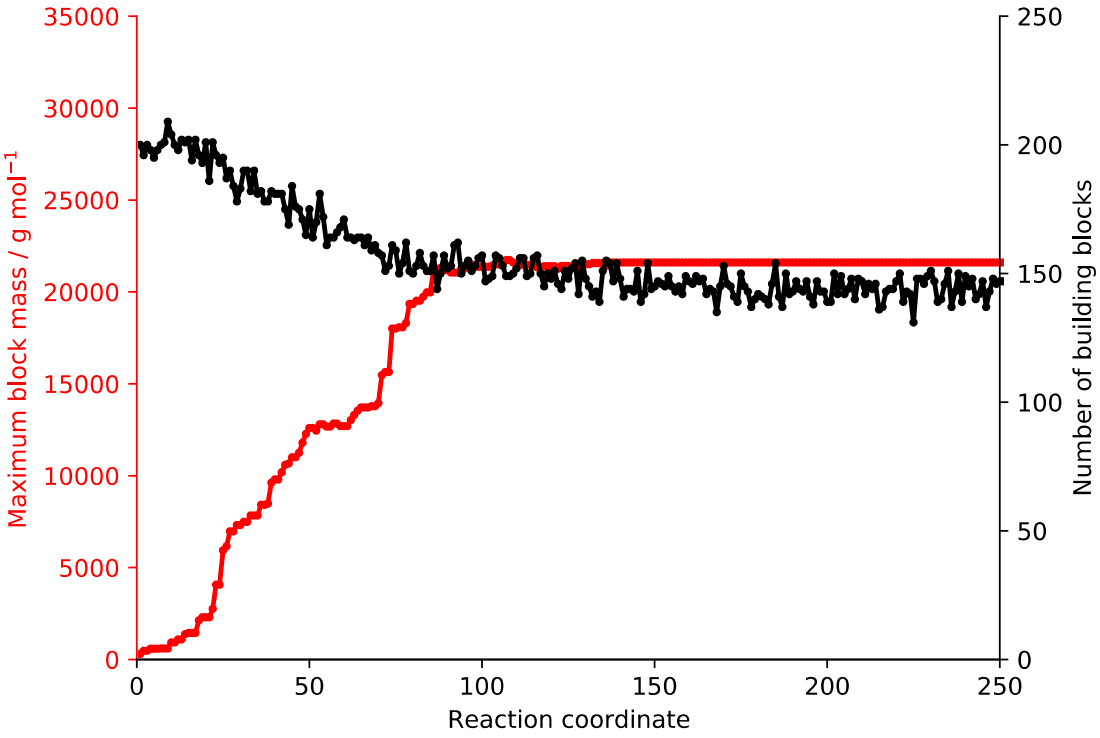
Maximum block mass / g mol⁻¹
Number of building blocks
Reaction coordinate
0
5000
10000
15000
20000
25000
30000
35000
0
50
100
150
200
250

b)

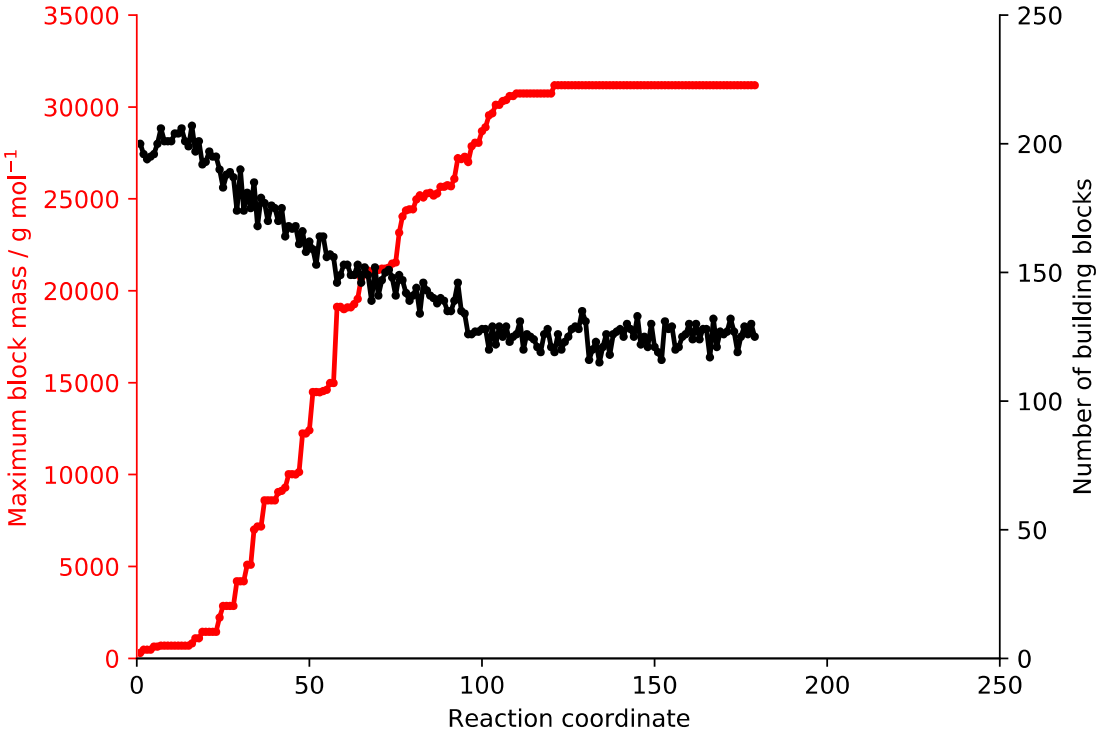
Maximum block mass / g mol⁻¹
Number of building blocks
Reaction coordinate
0
5000
10000
15000
20000
25000
30000
35000
0
50
100
150
200
250

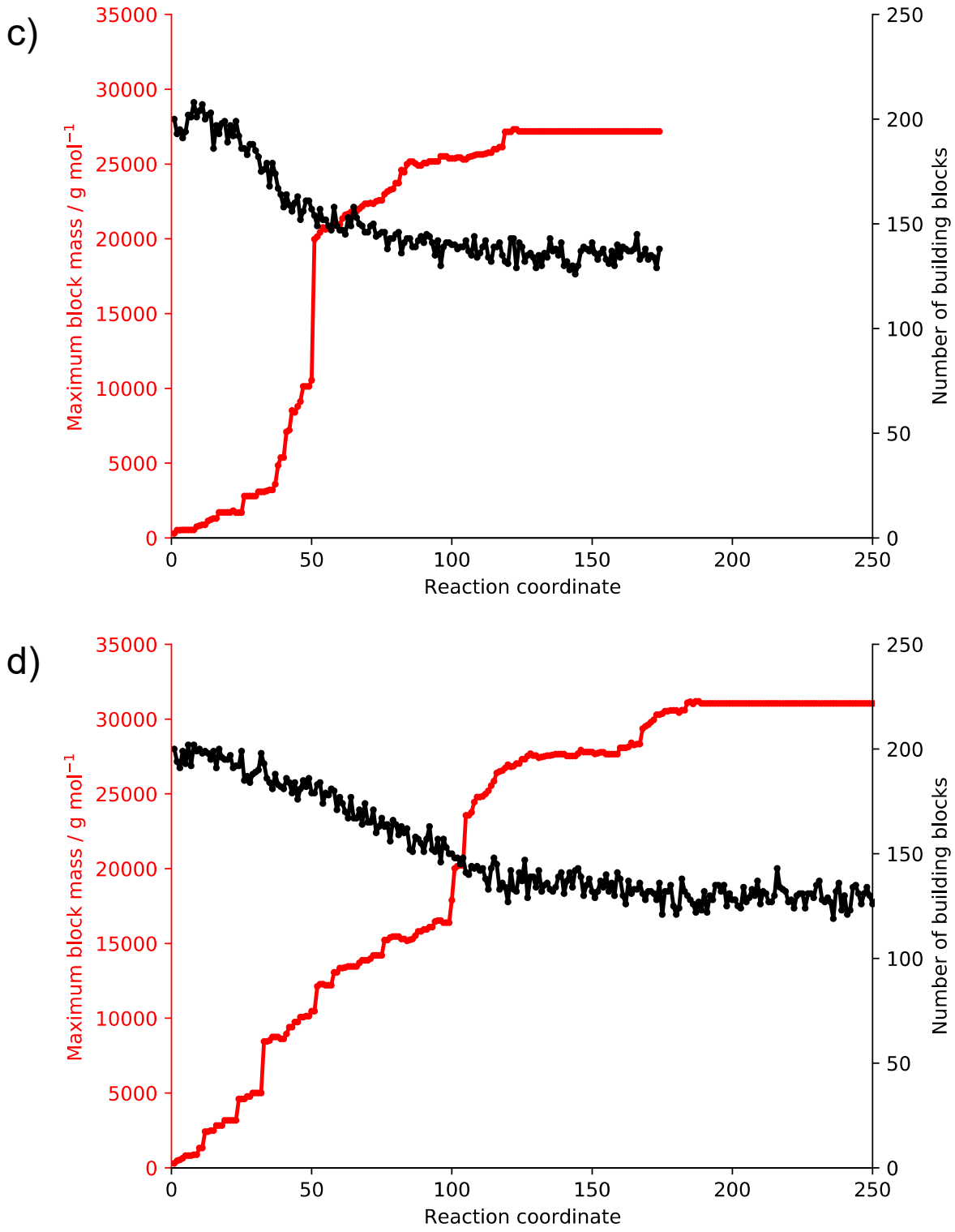

Figure S21. Plots of the maximum block size and number of blocks in the simulation cell against the reaction step for hybrid coarse-grain models 1–4, artificially synthesised using DMF as the solvent and using the fitted pair potentials given in Table S5: a) model 1, b) model 2, c) model 3, d) model 4. Key: Number of building blocks – black, maximum block mass – red.

9. Porosity analysis

Table S6. Comparison of the average porosity properties of the small CMP–1 networks artificially synthesised in DMF (AA) and toluene (CG) using the all-atom and hybrid coarse-grain techniques. Included as a benchmark are the porosity properties for the all-atom CMP–1 networks generated in DMF solvent as part of our previous work.[1] Surface area – network accessible surface area, micropore volume – network accessible helium volume. It is worth noting that whilst the average surface area and micropore volumes of the hybrid coarse-grain systems generated with fitted pair potentials in toluene solvent are larger than the all-atom equivalent, this is within the error of the surface area calculation, and the average value of across a relatively small number of models, so we would expect that on repeating this measurement across a larger dataset, we would see the average surface area of the hybrid coarse-grain system reduce to a lower value than the all-atom.

System	Solvent	PLD / Å	MPD / Å	Micropore volume / $cm^3\ g^{-1}$	Surface Area / $m^2\ g^{-1}$	Density / $g\ cm^{-3}$	Size of Initial Cell / %
Benchmark	DMF	6.00	11.50	0.74	1561	0.68	80.57
All-atom	DMF	8.34	13.55	1.34	3006	0.55	76.86
Hybrid coarse-grain (original pair parameters)	DMF	7.35	14.04	0.99	2200	0.67	90.25
Hybrid coarse-grain (fitted pair parameters)	DMF	5.55	10.96	0.75	1529	0.78	90.12
All-atom	Toluene	7.65	13.75	1.21	2843	0.55	78.51
Hybrid coarse-grain (original pair parameters)	Toluene	6.97	13.63	1.03	2361	0.65	86.23
Hybrid coarse-grain (fitted pair parameters)	Toluene	7.99	14.82	1.27	2900	0.59	90.66

Table S7. Comparison of the average elemental analysis properties of the small CMP–1 networks artificially synthesised in DMF (AA) and toluene (CG) using the all-atom and hybrid coarse-grain techniques. Included as a benchmark are the porosity properties for the all-atom CMP–1 networks generated as part of our previous work.[1]

System	Solvent	wt% C	wt% H	wt% P	wt% Cu	wt% Br	wt% Pd	wt% Other
Benchmark	DMF	78.34	2.73	0.93	5.00	11.11	1.85	19.19
All-atom	DMF	83.03	3.11	1.23	0.86	9.66	2.11	0.00
Hybrid coarse-grain (original pair parameters)	DMF	83.89	0.26	0.82	0.48	13.14	1.41	0.00
Hybrid coarse-grain (fitted pair parameters)	DMF	84.60	0.22	0.74	0.60	12.56	1.27	0.01
All-atom	Toluene	84.18	3.15	0.95	0.79	9.30	1.62	0.01
Hybrid coarse-grain (original pair parameters)	Toluene	84.41	0.30	1.23	0.72	11.23	2.11	0.00
Hybrid coarse-grain (fitted pair parameters)	Toluene	84.82	0.26	1.08	1.01	10.96	1.86	0.01

10. Mapping polymer fragments

Table S8. Summary of the building block connectivity in the small polymer fragments generated as part of the CG mapping process.

System	Block									
	1	2	3	4	5	6	7	8	9	10
1	DBB	cat								
2	TEB	cat								
3	DBB	TEB								
4	DBB	TEB	DBB							
5	TEB	DBB	TEB							
6	DBB	cat	DBB							
7	TEB	cat	TEB							
8	DBB	cat	DBB	TEB						
9	TEB	cat	TEB	DBB						
10	cat	DBB	cat	DBB						
11	cat	TEB	cat	TEB						
12	DBB	TEB	cat	TEB	DBB					
13	DBB	cat	DBB	cat	DBB					
14	TEB	cat	TEB	cat	TEB					
15	DBB	TEB	DBB	cat	DBB	TEB				
16	TEB	DBB	TEB	cat	TEB	DBB				
17	TEB	DBB	cat	DBB	cat	DBB				
18	DBB	cat	DBB	TEB	cat	TEB	DBB			
19	TEB	cat	TEB	DBB	cat	DBB	TEB			
20	cat	DBB	cat	DBB	TEB	DBB	TEB			
21	DBB	TEB	cat	TEB	DBB	cat	DBB	TEB		
22	TEB	cat	TEB	cat	TEB	DBB	TEB	DBB		
23	DBB	TEB	DBB	cat	DBB	TEB	cat	TEB		
24	TEB	cat	TEB	DBB	cat	DBB	TEB	DBB	TEB	
25	DBB	cat	DBB	TEB	cat	TEB	DBB	TEB	DBB	
26	DBB	TEB	DBB	cat	DBB	TEB	DBB	cat	DBB	
27	DBB	TEB	DBB	cat	DBB	TEB	cat	TEB	DBB	TEB
28	TEB	DBB	TEB	cat	TEB	DBB	cat	DBB	TEB	DBB
29	TEB	cat	TEB	cat	TEB	DBB	TEB	DBB	TEB	DBB

Figure S22. Structure of the all-atom (left) and mapped coarse-grain (right) polymer fragment 1. Key: C – grey, H – white, Pd – dim blue, P – purple, BER grain – red, Br – burgundy, dBER grain – pale blue.

Figure S23. Structure of the all-atom (left) and mapped coarse-grain (right) polymer fragment 2. Key: C – grey, H – white, Cu – orange, tBER grain – bright blue, Pd – dim blue, P – purple, BER grain – red.

Figure S24. Structure of the all-atom (left) and mapped coarse-grain (right) polymer fragment 3. Key: C – grey, H – white, Cu – orange, tBER grain – bright blue, BER grain – red, Br – burgundy, dBER grain – pale blue.

Figure S25. Structure of the all-atom (left) and mapped coarse-grain (right) polymer fragment 4. Key: C – grey, H – white, Cu – orange, tBER grain – bright blue, BER grain – red, Br – burgundy, dBER grain – pale blue.

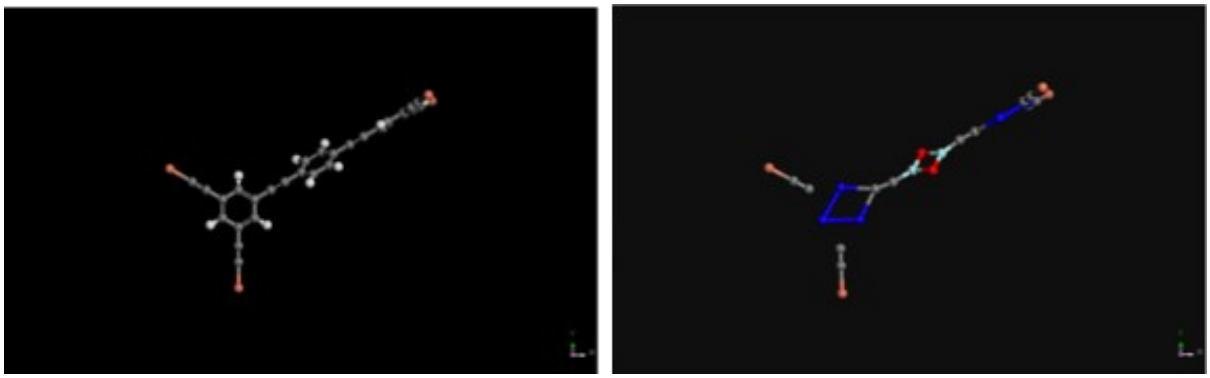

Figure S26. Structure of the all-atom (left) and mapped coarse-grain (right) polymer fragment 5. Key: C – grey, H – white, Cu – orange, tBER grain – bright blue, BER grain – red, dBER grain – pale blue.

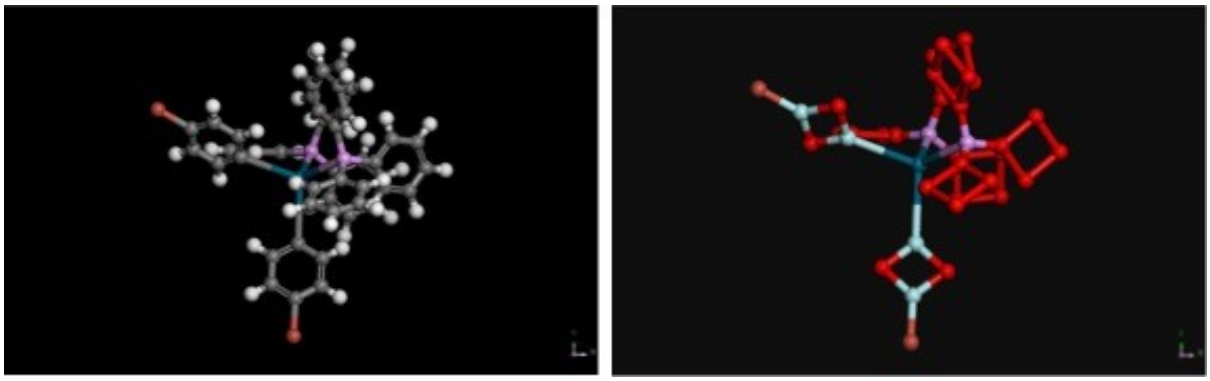

Figure S27. Structure of the all-atom (left) and mapped coarse-grain (right) polymer fragment 6. Key: C – grey, H – white, Pd – dim blue, P – purple, BER grain – red, Br – burgundy, dBER grain – pale blue.

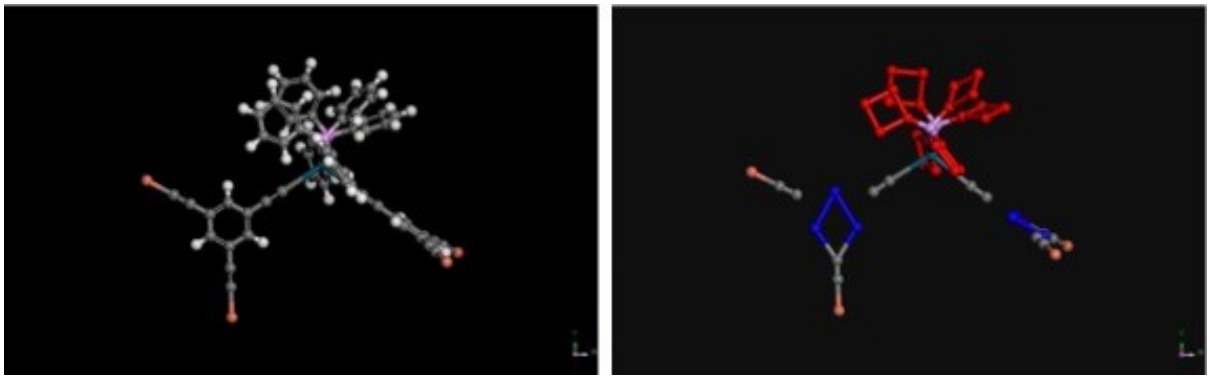

Figure S28. Structure of the all-atom (left) and mapped coarse-grain (right) polymer fragment 7. Key: C – grey, H – white, Cu – orange, tBER grain – bright blue, Pd – dim blue, P – purple, BER grain – red.

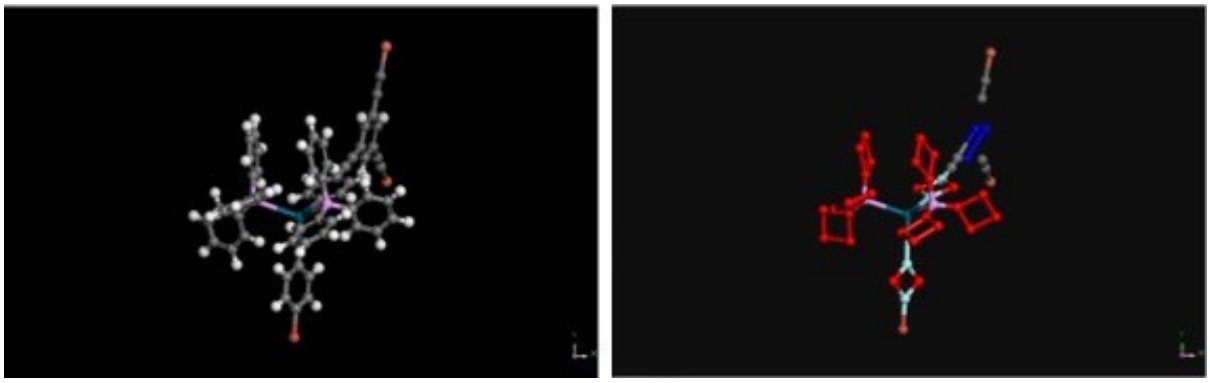

Figure S29. Structure of the all-atom (left) and mapped coarse-grain (right) polymer fragment 8. Key: C – grey, H – white, Cu – orange, tBER grain – bright blue, Pd – dim blue, P – purple, BER grain – red, Br – burgundy, dBER grain – pale blue.

Figure S30. Structure of the all-atom (left) and mapped coarse-grain (right) polymer fragment 9. Key: C – grey, H – white, Cu – orange, tBER grain – bright blue, Pd – dim blue, P – purple, BER grain – red, Br – burgundy, dBER grain – pale blue.

Figure S31. Structure of the all-atom (left) and mapped coarse-grain (right) polymer fragment 10. Key: C – grey, H – white, Pd – dim blue, P – purple, BER grain – red, Br – burgundy, dBER grain – pale blue.

Figure S32. Structure of the all-atom (left) and mapped coarse-grain (right) polymer fragment 11. Key: C – grey, H – white, Cu – orange, tBER grain – bright blue, Pd – dim blue, P – purple, BER grain – red.

Figure S33. Structure of the all-atom (left) and mapped coarse-grain (right) polymer fragment 12. Key: C – grey, H – white, Cu – orange, tBER grain – bright blue, Pd – dim blue, P – purple, BER grain – red, Br – burgundy, dBER grain – pale blue.

Figure S34. Structure of the all-atom (left) and mapped coarse-grain (right) polymer fragment 13. Key: C – grey, H – white, Pd – dim blue, P – purple, BER grain – red, Br – burgundy, dBER grain – pale blue.

Figure S35. Structure of the all-atom (left) and mapped coarse-grain (right) polymer fragment 14. Key: C – grey, H – white, Cu – orange, tBER grain – bright blue, Pd – dim blue, P – purple, BER grain – red.

Figure S36. Structure of the all-atom (left) and mapped coarse-grain (right) polymer fragment 15. Key: C – grey, H – white, Cu – orange, tBER grain – bright blue, Pd – dim blue, P – purple, BER grain – red, Br – burgundy, dBER grain – pale blue.

Figure S37. Structure of the all-atom (left) and mapped coarse-grain (right) polymer fragment 16. Key: C – grey, H – white, Cu – orange, tBER grain – bright blue, Pd – dim blue, P – purple, BER grain – red, Br – burgundy, dBER grain – pale blue.

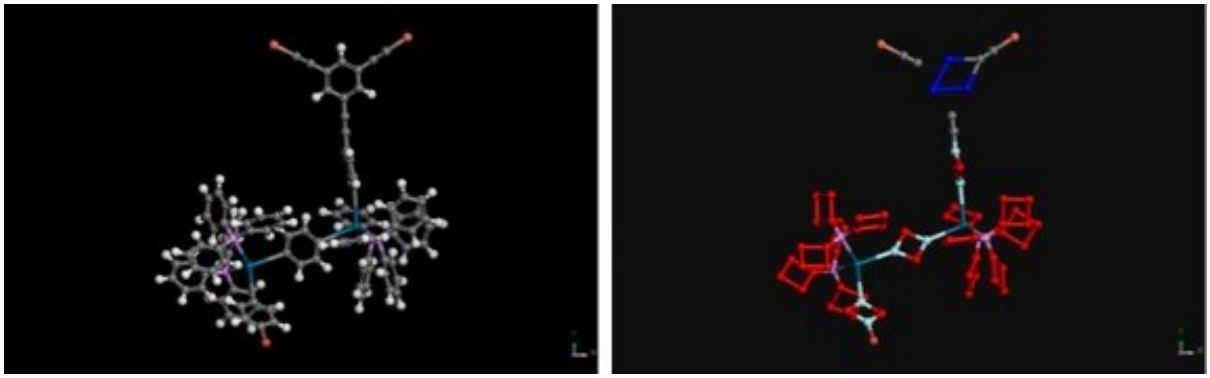

Figure S38. Structure of the all-atom (left) and mapped coarse-grain (right) polymer fragment 17. Key: C – grey, H – white, Cu – orange, tBER grain – bright blue, Pd – dim blue, P – purple, BER grain – red, Br – burgundy, dBER grain – pale blue.

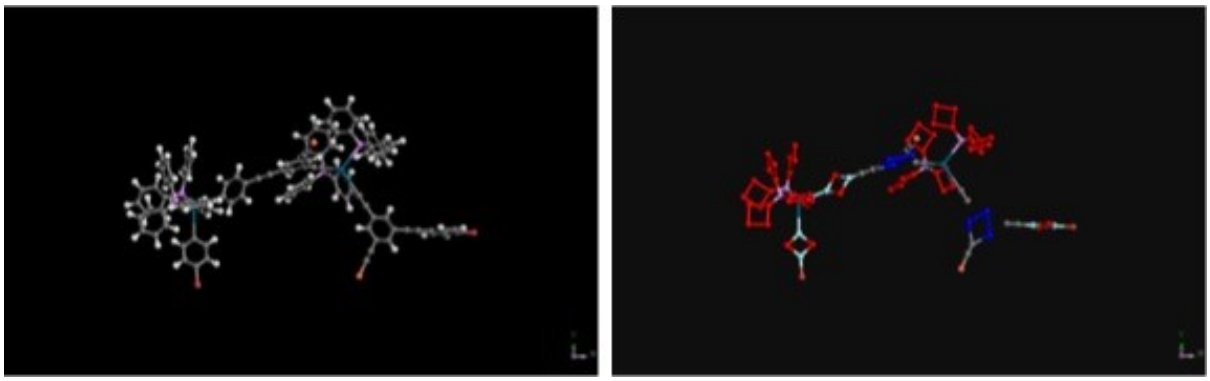

Figure S39. Structure of the all-atom (left) and mapped coarse-grain (right) polymer fragment 18. Key: C – grey, H – white, Cu – orange, tBER grain – bright blue, Pd – dim blue, P – purple, BER grain – red, Br – burgundy, dBER grain – pale blue.

Figure S40. Structure of the all-atom (left) and mapped coarse-grain (right) polymer fragment 19. Key: C – grey, H – white, Cu – orange, tBER grain – bright blue, Pd – dim blue, P – purple, BER grain – red, dBER grain – pale blue.

Figure S41. Structure of the all-atom (left) and mapped coarse-grain (right) polymer fragment 20. Key: C – grey, H – white, Cu – orange, tBER grain – bright blue, Pd – dim blue, P – purple, BER grain – red, dBER grain – pale blue.

Figure S42. Structure of the all-atom (left) and mapped coarse-grain (right) polymer fragment 21. Key: C – grey, H – white, Cu – orange, tBER grain – bright blue, Pd – dim blue, P – purple, BER grain – red, Br – burgundy, dBER grain – pale blue.

Figure S43. Structure of the all-atom (left) and mapped coarse-grain (right) polymer fragment 22. Key: C – grey, H – white, Cu – orange, tBER grain – bright blue, Pd – dim blue, P – purple, BER grain – red, Br – burgundy, dBER grain – pale blue.

Figure S44. Structure of the all-atom (left) and mapped coarse-grain (right) polymer fragment 23. Key: C – grey, H – white, Cu – orange, tBER grain – bright blue, Pd – dim blue, P – purple, BER grain – red, Br – burgundy, dBER grain – pale blue.

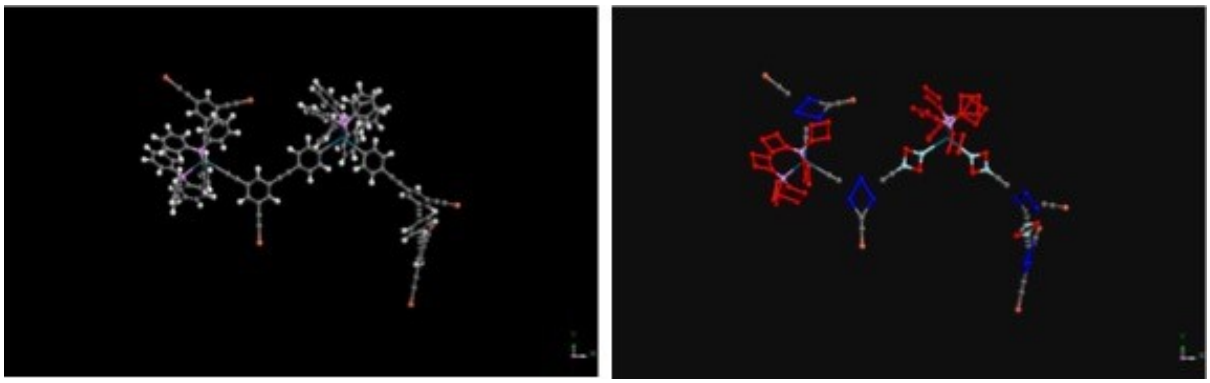

Figure S45. Structure of the all-atom (left) and mapped coarse-grain (right) polymer fragment 24. Key: C – grey, H – white, Cu – orange, tBER grain – bright blue, Pd – dim blue, P – purple, BER grain – red, dBER grain – pale blue.

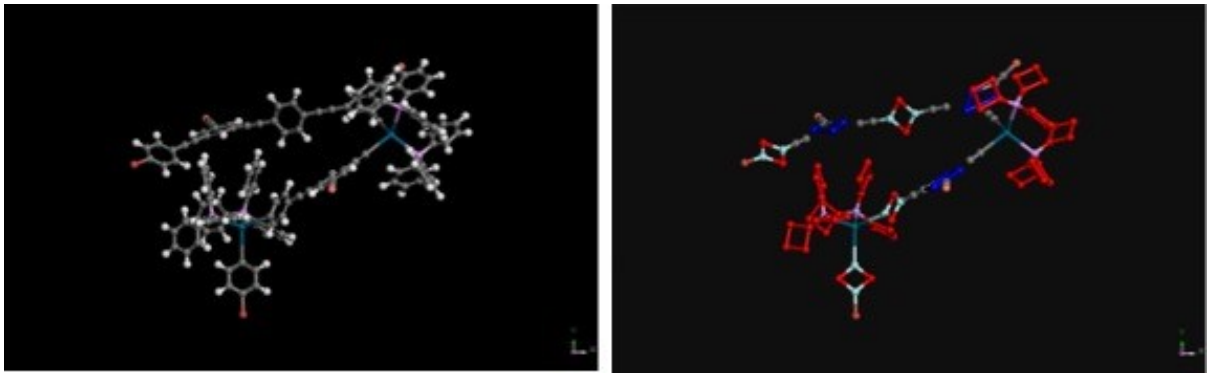

Figure S46. Structure of the all-atom (left) and mapped coarse-grain (right) polymer fragment 25. Key: C – grey, H – white, Cu – orange, tBER grain – bright blue, Pd – dim blue, P – purple, BER grain – red, Br – burgundy, dBER grain – pale blue.

Figure S47. Structure of the all-atom (left) and mapped coarse-grain (right) polymer fragment 26. Key: C – grey, H – white, Cu – orange, tBER grain – bright blue, Pd – dim blue, P – purple, BER grain – red, Br – burgundy, dBER grain – pale blue.

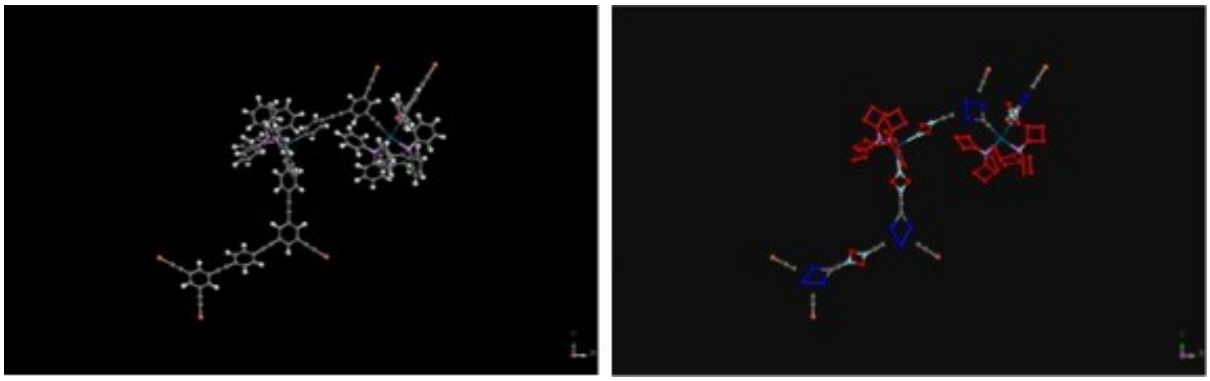

Figure S48. Structure of the all-atom (left) and mapped coarse-grain (right) polymer fragment 27. Key: C – grey, H – white, Cu – orange, tBER grain – bright blue, Pd – dim blue, P – purple, BER grain – red, Br – burgundy, dBER grain – pale blue.

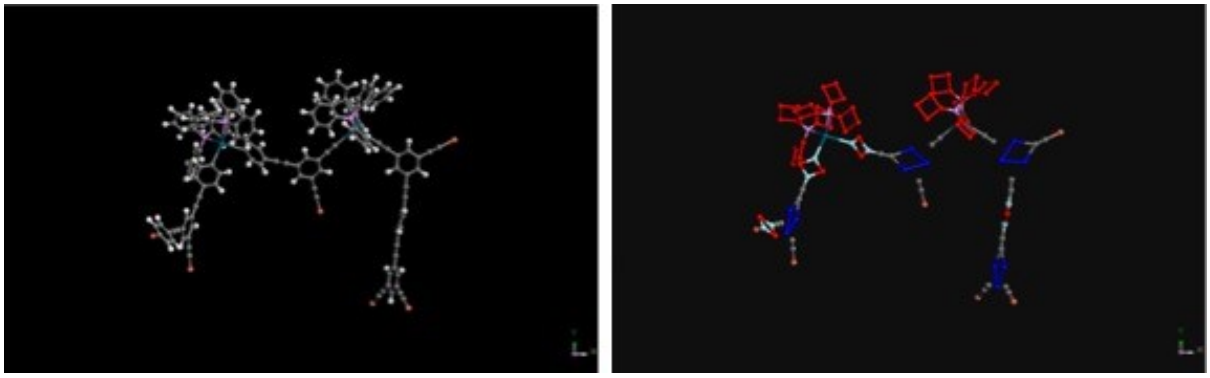

Figure S49. Structure of the all-atom (left) and mapped coarse-grain (right) polymer fragment 28. Key: C – grey, H – white, Cu – orange, tBER grain – bright blue, Pd – dim blue, P – purple, BER grain – red, Br – burgundy, dBER grain – pale blue.

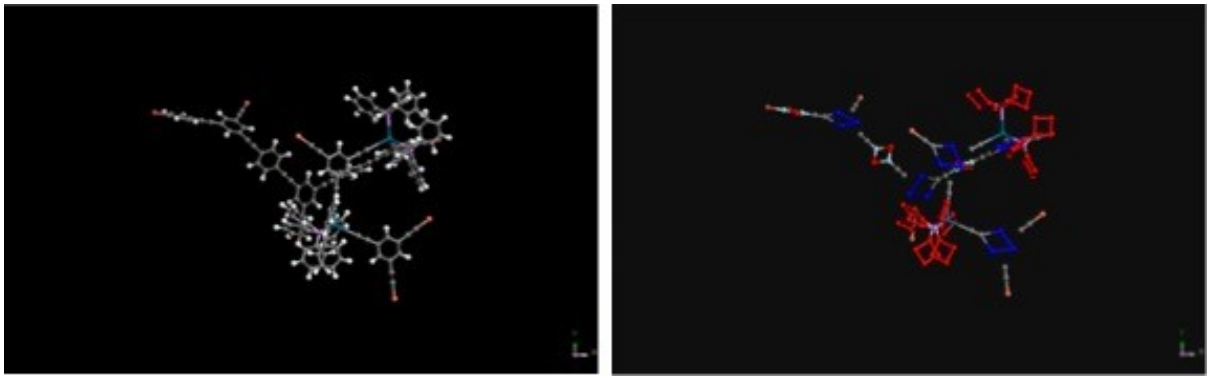

Figure S50. Structure of the all-atom (left) and mapped coarse-grain (right) polymer fragment 29. Key: C – grey, H – white, Cu – orange, tBER grain – bright blue, Pd – dim blue, P – purple, BER grain – red, Br – burgundy, dBER grain – pale blue.

Table S9. Comparison of the porosity properties of the small CMP–1 polymer fragments generated in the absence of solvent using the all-atom and mapped hybrid coarse-grain techniques. Surface area – network accessible surface area, micropore volume – network accessible helium volume. Relative surface areas and micropore volumes are normalised so that the atomistic values for each system number are set to 100%. Whilst these surface areas and micropore volumes appear very large, this is simply due to the systems being in a very large simulation cell to make the mapping process easier.

	All atom		Coarse-grained		Coarse-grained relative to all atom	
System	Surface Area / $m^2\ g^{-1}$	Micropore Volume / $cm^3\ g^{-1}$	Surface Area / $m^2\ g^{-1}$	Micropore Volume / $cm^3\ g^{-1}$	Surface Area / %	Micropore Volume / %
1	8753	764.366	6627	615.747	76	81
2	8780	664.534	7481	562.089	85	85
3	10207	1400.113	9799	1305.985	96	93
4	10367	1152.498	9492	1035.570	92	90
5	10654	964.381	10099	914.585	95	95
6	7756	638.633	6009	518.621	77	81
7	8642	510.457	7276	446.751	84	88
8	8491	529.416	6718	443.211	79	84
9	8829	473.337	7404	410.080	84	87
10	7231	402.572	5375	320.911	74	80
11	8270	344.274	6750	289.536	82	84
12	9065	441.247	7521	378.976	83	86
13	7428	364.723	5519	292.352	74	80
14	7849	297.659	6628	255.505	84	86
15	8827	422.714	7251	359.119	82	85
16	9195	386.171	7732	337.046	84	87
17	7779	326.240	6024	266.735	77	82
18	8198	290.442	6559	242.024	80	83
19	8361	276.793	6901	234.729	83	85
20	8530	304.458	6721	251.673	79	83
21	8528	265.486	7045	224.182	83	84
22	8045	250.563	6669	215.355	83	86
23	8539	265.487	7115	224.182	83	84
24	8760	244.475	7320	208.791	84	85
25	7778	255.052	6453	214.532	83	84
26	8339	270.531	6722	223.292	81	83
27	8717	235.610	7283	200.404	84	85
28	8777	235.610	7277	200.405	83	85
29	8754	223.786	7440	193.325	85	86

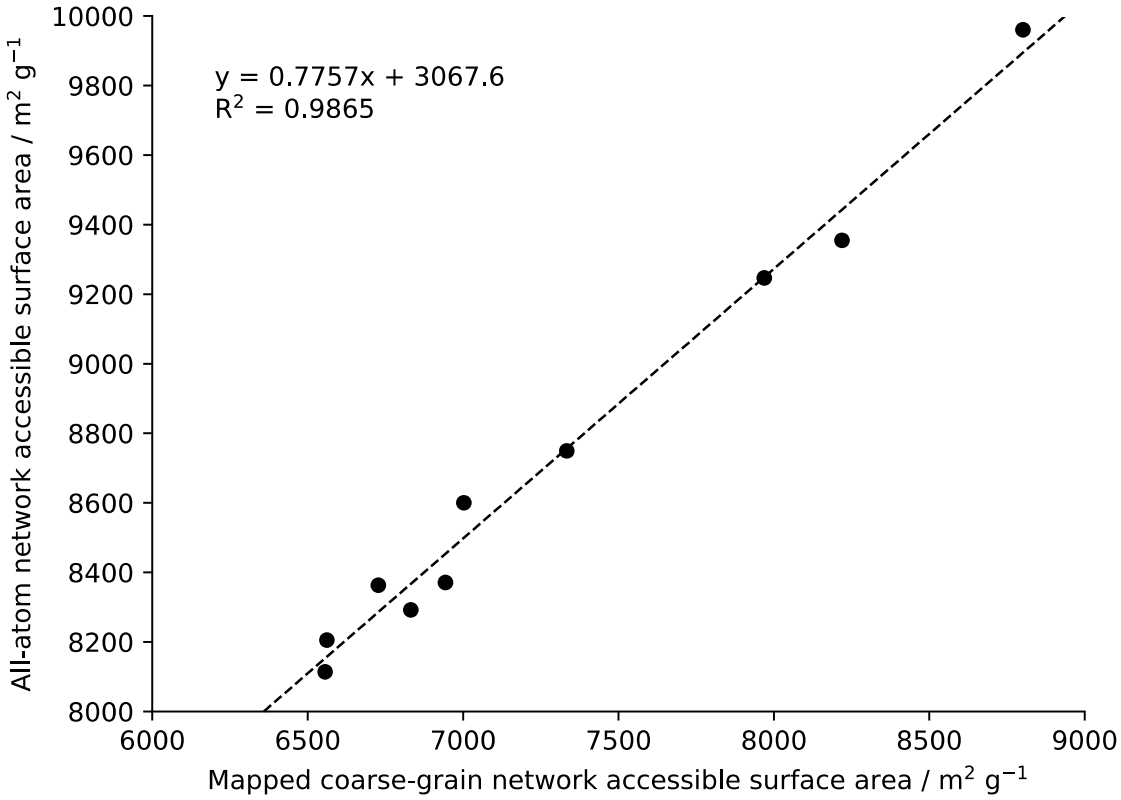

Figure S51. Plot of the mapped coarse-grain network accessible surface area against the all-atom network accessible surface area for each polymer fragment size. For each fragment size, the surface areas of the respective set are averaged. The line of best fit dictates a shift factor that could be employed to determine the all-atom surface area from a hybrid coarse-grain model prepared using the approaches described in this work.

11. Reaction scale-up

Table S10. Number of building blocks within the simulation cell at each unit cell length.

Building block	Cell length / Å						
	50	75	100	125	150	175	200
Catalyst	4	14	32	63	108	172	256
TEA	70	236	560	1094	1890	3001	4480
DBB	100	338	800	1563	2700	4288	6400
TEB	100	338	800	1563	2700	4288	6400
Toluene	130	439	1040	2031	3510	5574	8320
Cell volume / $Å^3$	125000	421875	1000000	1953125	3375000	5359375	8000000
Scale factor from (50,50,50) cell	1.000	3.375	8.000	15.625	27.000	42.875	64.000

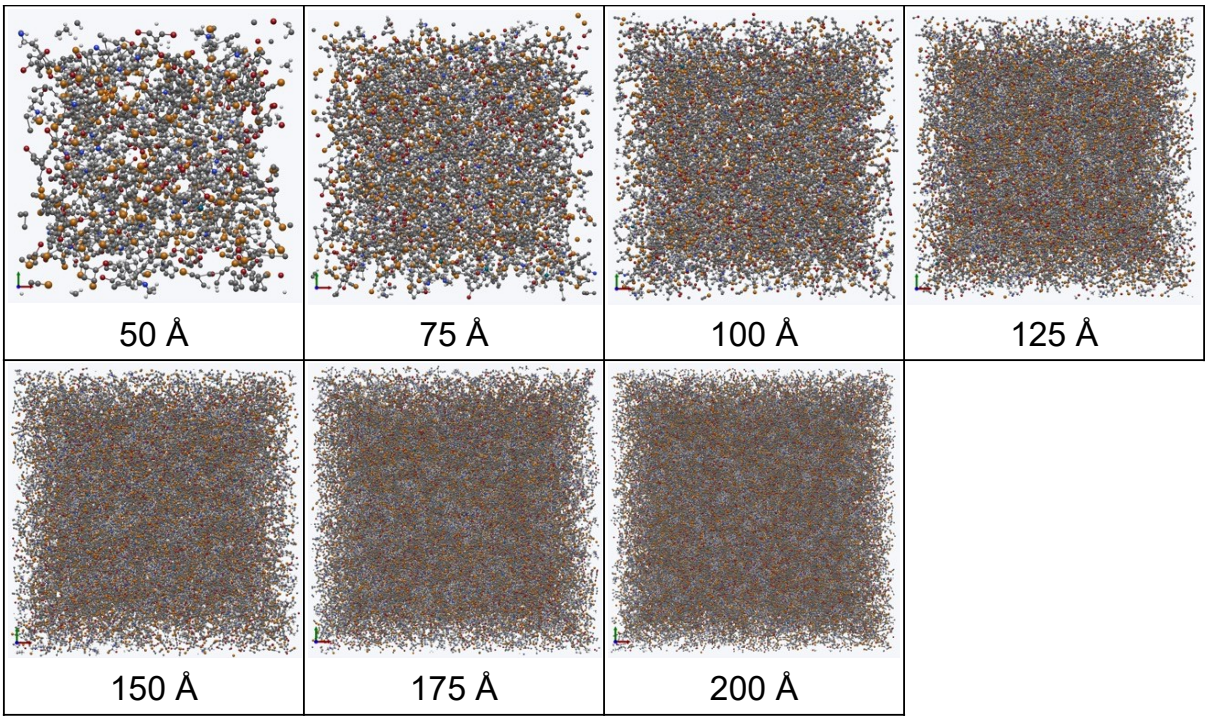

Figure S52. Structure of each of the scaled-up models artificially synthesised in toluene solvent and their respective cell lengths.

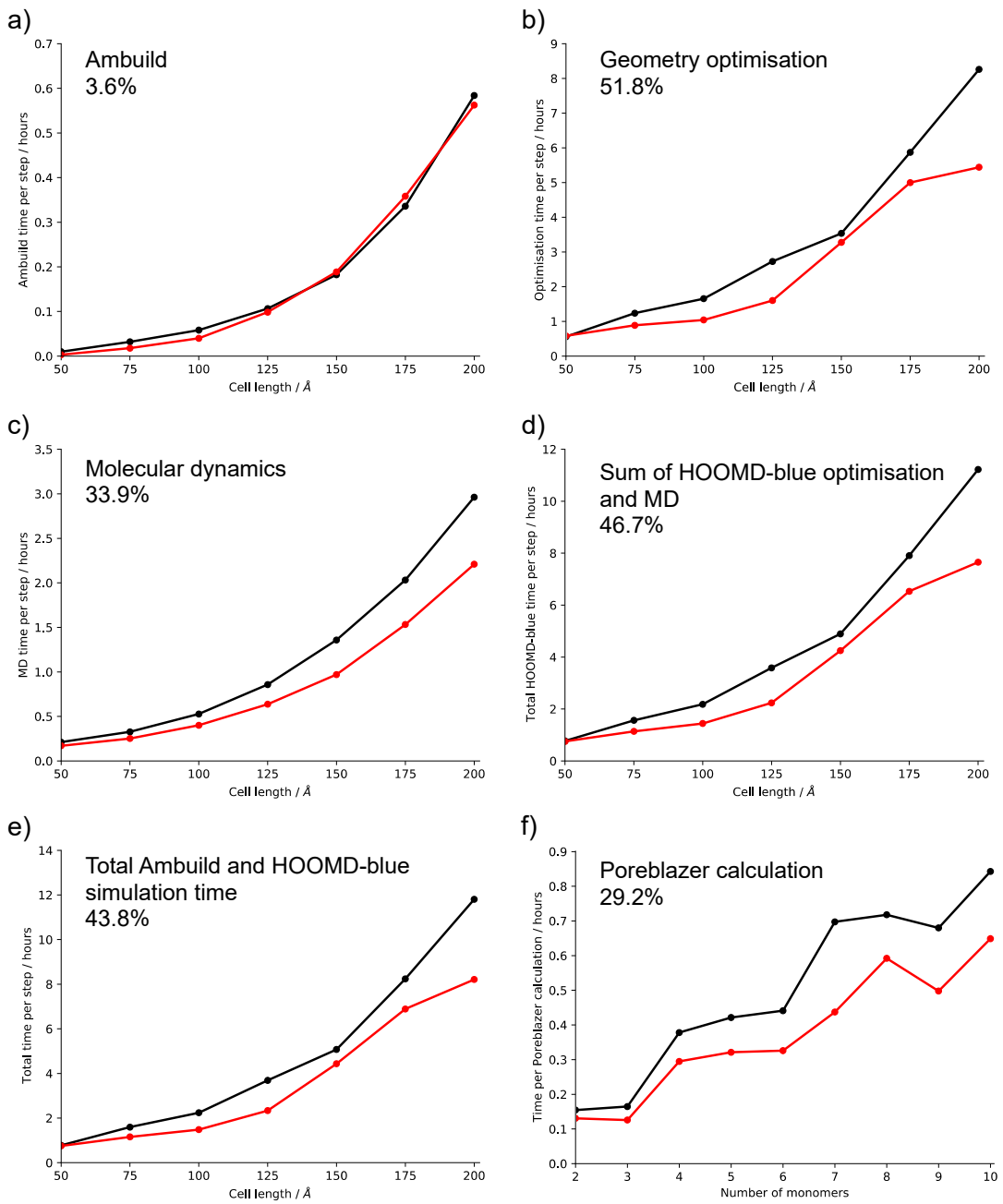

Figure S53. a) – e) Plots of the unit cell length against the simulation time elapsed per step for steps 1–2 of the CMP–1 network formation process. a) Ambuild simulation time, b) HOOMD-blue geometry optimisation simulation time, c) HOOMD-blue MD simulation time, d) total HOOMD-blue geometry optimisation and molecular dynamics simulation time, e) total Ambuild and HOOMD-blue simulation time. f) plot of the number of monomers in the small fragments against the Poreblazer calculation time. Key: all-atom – black, hybrid coarse-grain – red. The percentage speed-up reported on each plot was calculated using the formula:

$$Percentage\ speed-up = \frac{AA\ time - CG\ time}{CG\ time}\ x\ 100$$

Where the maximum percentage speed-up is seen at the largest cell length of 200 Å.

Scaled-up artificial synthesis

The methodology used in the artificial synthesis process for the scaled-up model had to be adapted due to the system size. The network generation procedure remained largely the same, however it was necessary, due to the number of molecules within our simulation cell, to reduce the timestep, temperature factor, and van der Waals cut-off to enable the structure to perform any geometry optimisation or molecular dynamics. The temperature factor was set to 1.0, the timestep was set to 0.000005 ps, and the van der Waals cut-off set to 1.0. To prevent the simulation crashing on attempting to form a very large number of bonds at the same time due to the increased number of building blocks within close proximity to each other in the unit cell giving rise to too many competing forces all trying to optimise at the same time on forming the new bonds, we began with a smaller zip step bond length of 6, retaining the bond angle at 90, meaning that monomers within a cone of length 6 Å and radius 90° from the catalyst, and from two monomer building blocks both bonded to a catalyst molecule would be able to react. This reduced the number of bonds that were able to form in the first instance, which helped to stabilise the system and allow the simulation to continue. Then, once the system had stabilised and we were seeing a reduction in the number of new bonds forming, we gradually increased the zip step bond length in increments of 1 Å until we reached the bond length of 10 used in the smaller systems (Figure S54).

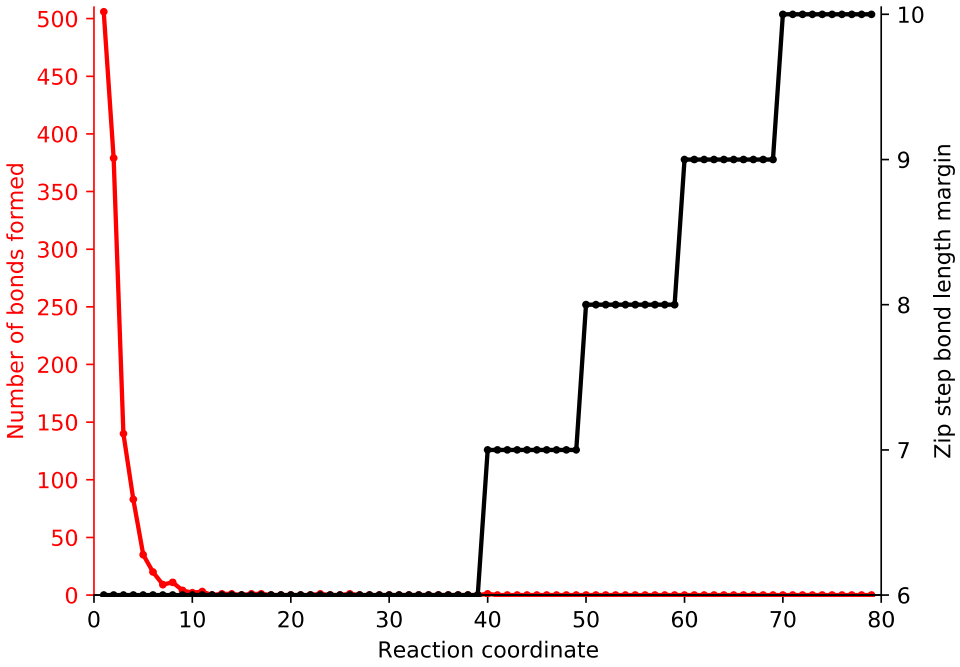

Figure S54. Plots of the number of bonds formed and zip step bond length margin in the scaled-up simulation cell against the reaction step, artificially synthesised using toluene as the solvent. Key: Number of bonds formed – red, zip step bond length margin – black.

The desolvation protocol was also adjusted to add in more NPT molecular dynamics throughout, whereby after each of the network generation, desolvation and homocoupling stages, an extra optimisation and NPT loop was incorporated to allow the cell dimensions and forces to equilibrate throughout. Once the desolvation was complete, and all solvent and unreacted building blocks had been removed from the cell, leaving significantly fewer building blocks to consider, we increased the van der Waals cut-off value to 10, and reduced the temperature factor to 0.01, so that more interactions between particles were considered by increasing the van der Waals cut-off, and by lowering the temperature factor, we essentially optimised the structure whilst giving it some energy to move and optimise the cell dimensions. Then, on reaching the homocoupling, we replaced the NPT MD within the homocoupling cycle with NVT MD, and instead added in the NPT MD later, once the homocoupling was complete. To begin with, we tightened the criteria required in the bond and bond angle criteria required to form a zip step within the homocoupling and final cell equilibration loop by reducing the bond length to 2 and the bond angle to 70, before gradually increasing these back to the values of 8 Å and 90° as used in the smaller systems. This approach slowed the rate of new bond formation, which helped to minimise the competing forces within the cell on forming multiple bonds at the same time.

The cell length of the scaled unit cell throughout the desolvation, homocoupling, workup, and cell equilibration protocol is plotted in Figure S55 as a function of the reaction coordinate. It can be seen that the cell length initially increases during the first cycle of NPT (after network generation, orange), indicating that the cell swells in order to minimise the multiple competing forces and large number of building blocks within the system. Then, once we start to remove solvent and unreacted building blocks during the desolvation protocol, the cell length rapidly decreases (green) to below the original cell length of 200 Å. The cell length increases once more at the beginning of the NPT after desolvation (purple) as more interactions between building blocks are considered once the van der Waals cut-off value is increased back to the original value of 10 (used in the smaller models with cell length of 50 Å), but once this change has occurred, the cell length then continues to decrease throughout the remaining NPT steps, with a sharp decrease during the NPT after homocoupling (yellow) as the added alkyne-alkyne bonds help to draw the polymer cluster together, and a steady decrease in cell length during the final cell equilibration after the workup (blue), once all unreacted copper end groups are replaced with hydrogen atoms.

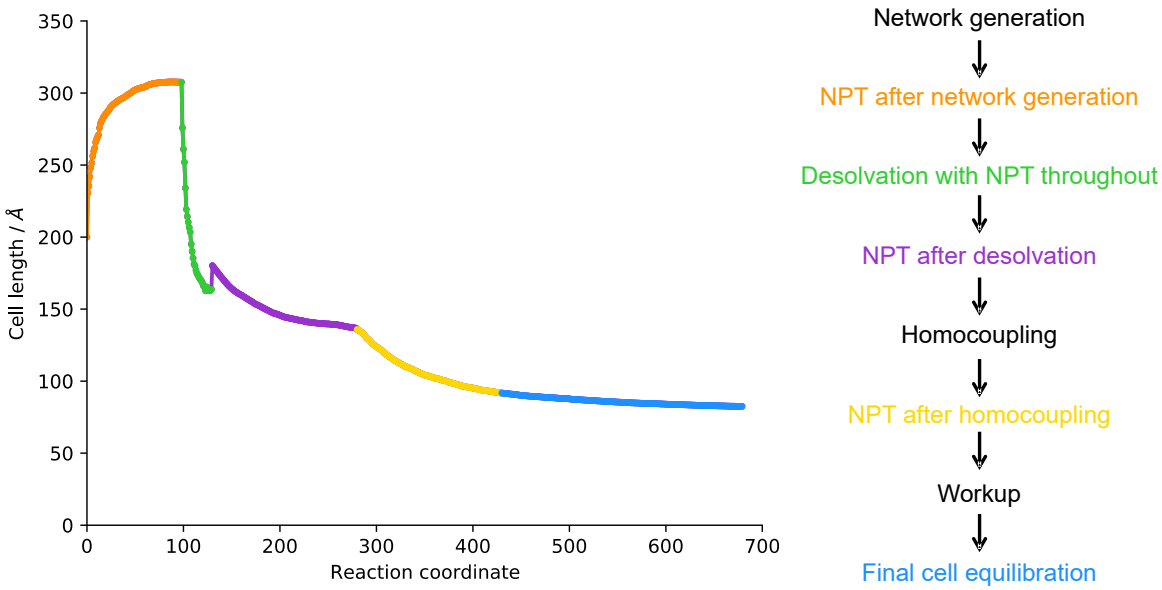

Figure S55. Plot of the scaled unit cell length during the desolvation, homocoupling, workup, and cell equilibration as a function of the reaction coordinate (left) and flow chart of the artificial synthesis of the scaled unit cell (right). Key: NPT after network generation – orange, NPT throughout desolvation – green, NPT after desolvation – purple (initial increase due to increase in rCut), NPT after homocoupling – yellow, and final cell equilibration – blue.

Table S11. Comparison of the average porosity properties of the CMP–1 networks artificially synthesised in toluene using the hybrid coarse-grain technique at the original and scaled up cell sizes. Surface area – network accessible surface area, micropore volume – network accessible helium volume.

System	Cell length / Å	PLD / Å	MPD / Å	Micropore volume / $cm^3\ g^{-1}$	Surface Area / $m^2\ g^{-1}$	Density / $g\ cm^{-3}$	Size of Initial Cell / %
Original cell size	50	6.97	13.63	1.03	2361	0.65	86.23
Scaled cell size	200	3.25	12.26	0.26	286	1.16	82.48

Table S12. Comparison of the average elemental analysis properties of the CMP–1 networks artificially synthesised in toluene using the hybrid coarse-grain technique at the original and scaled up cell sizes.

System	Cell length / Å	wt% C	wt% H	wt% P	wt% Cu	wt% Br	wt% Pd	wt% Other
Original cell size	50	84.41	0.30	1.23	0.72	11.23	2.11	0.00
Scaled cell size	200	65.34	0.00	6.29	4.49	13.07	10.81	0.00

12. Additional references

1. J. M. H. Thomas, C. Mollart, L. Turner, P. Heasman, P. Fayon and A. Trewin, *J. Phys. Chem. B*, 2020, **124**, 7318-7326.
2. P. Fayon, J. M. H. Thomas and A. Trewin, *J. Phys. Chem. C*, 2016, **120**, 25880-25891.
3. C. Mollart, S. Holcroft, M. J. G. Peach, A. Rowling and A. Trewin, *Phys. Chem. Chem. Phys.*, 2022, **24**, 20025-20029.
4. J. M. H. Thomas and A. Trewin, *J. Phys. Chem. C*, 2014, **118**, 19712-19722.
5. A. Laybourn, R. Dawson, R. Clowes, T. Hasell, A. I. Cooper, Y. Z. Khimyak and D. J. Adams, *Polym. Chem.*, 2014, **5**, 6325-6333.
6. D. Berthelot, *Comptes rendus hebdomadaires des séances de l'Académie des Sciences*, 1898, **126**, 1703-1855.
7. H. A. Lorentz, *Annalen der Physik*, 1881, **248**, 127-136.
8. R. DeVane, M. L. Klein, C.-c. Chiu, S. O. Nielsen, W. Shinoda and P. B. Moore, *J. Phys. Chem. B*, 2010, **114**, 6386-6393.